Cellular and Molecular Life Sciences (2023) 80:371
https://doi.org/10.1007/s00018-023-05022-0

ORIGINAL ARTICLE

Recombinant protein delivery enables modulation of the phototransduction cascade in mouse retina

Sabrina Asteriti[1,2] · Valerio Marino[1] · Anna Avesani[1] · Amedeo Biasi[1] · Giuditta Dal Cortivo[1] · Lorenzo Cangiano[2] · Daniele Dell'Orco[1]

Received: 24 July 2023 / Revised: 10 October 2023 / Accepted: 27 October 2023

Abstract

Inherited retinal dystrophies are often associated with mutations in the genes involved in the phototransduction cascade in photoreceptors, a paradigmatic signaling pathway mediated by G protein-coupled receptors. Photoreceptor viability is strictly dependent on the levels of the second messengers cGMP and Ca^{2+}. Here we explored the possibility of modulating the phototransduction cascade in mouse rods using direct or liposome-mediated administration of a recombinant protein crucial for regulating the interplay of the second messengers in photoreceptor outer segments. The effects of administration of the free and liposome-encapsulated human guanylate cyclase-activating protein 1 (GCAP1) were compared in biological systems of increasing complexity (in cyto, ex vivo, and in vivo). The analysis of protein biodistribution and the direct measurement of functional alteration in rod photoresponses show that the exogenous GCAP1 protein is fully incorporated into the mouse retina and photoreceptor outer segments. Furthermore, only in the presence of a point mutation associated with cone-rod dystrophy in humans p.(E111V), protein delivery induces a disease-like electrophysiological phenotype, consistent with constitutive activation of the retinal guanylate cyclase. Our study demonstrates that both direct and liposome-mediated protein delivery are powerful complementary tools for targeting signaling cascades in neuronal cells, which could be particularly important for the treatment of autosomal dominant genetic diseases.

Keywords Protein therapy · Protein delivery · Inherited retinal dystrophy · Liposome · Cone dystrophy · Cone-rod dystrophy

Introduction

The molecular processes underlying vision are triggered by the absorption of photons by opsins in retinal photoreceptors. Located in specific membranous compartments in the outer segments of rods and cones, opsins are G protein-coupled receptors (GPCRs) that activate the signaling cascade known as phototransduction. For many years, phototransduction has been considered paradigmatic for the largest class of GPCR-mediated signaling pathways (rhodopsin-like or class-A GPCRs), and the accumulated knowledge about the structural, biochemical, and physiological details of this cascade has enabled significant advances in

Sabrina Asteriti and Valerio Marino have contributed equally to this work.

✉ Lorenzo Cangiano
lorenzo.cangiano@unipi.it

✉ Daniele Dell'Orco
daniele.dellorco@univr.it

Sabrina Asteriti
sabrina.asteriti@univr.it

Valerio Marino
valerio.marino@univr.it

Anna Avesani
anna.avesani@univr.it

Amedeo Biasi
amedeo.biasi@univr.it

Giuditta Dal Cortivo
giuditta.dalcortivo@univr.it

[1] Department of Neurosciences, Biomedicine and Movement Sciences, Section of Biological Chemistry, University of Verona, 37134 Verona, Italy

[2] Department of Translational Research, University of Pisa, 56123 Pisa, Italy

Published online: 25 November 2023

drug design and pharmacological approaches for many other signaling pathways [1, 2].

The phototransduction cascade converts the light signal detected by the opsins into a chemical signal, culminating in the transient fall of vesicular glutamate release from the photoreceptor synaptic terminal, which is sensed by downstream neurons [3]. Rods and cones adapt to dramatic changes in ambient light by modifying the kinetics of phototransduction, a finely regulated process orchestrated by the second messengers Ca^{2+} and cyclic guanosine monophosphate (cGMP). Absorption of light by rhodopsin (or cone opsins) triggers the hydrolysis of cGMP by activating the phosphodiesterase 6, thereby causing the dissociation of cGMP from cyclic nucleotide-gated channels (CNG) and their closure. The ensuing decrease in the inflow of Na^+ and Ca^{2+} hyperpolarizes the cell which, in turn, causes a reduction in neurotransmitter release. In parallel to these events, the light-independent extrusion of Ca^{2+} from the Na^+/Ca^{2+}, K^+-exchanger leads to a drop of Ca^{2+} concentration in the outer segments (from ~ 600 nM in the dark to below 100 nM in bright light [4]).

These light-evoked alterations of second messenger levels in the photoreceptor outer segment trigger feedback mechanisms necessary for the timely shutoff of the cascade, as well as for the adaptation to specific light or dark conditions [3, 5]. Subtle changes in Ca^{2+} concentration are promptly detected by guanylate cyclase-activating proteins (GCAPs), members of the neuronal calcium sensors family [6]. Two isoforms (GCAP1 and GCAP2) are expressed in rods and cones, but in human only GCAP1 seems to be actively involved in the phototransduction cascade as a modulator of retinal guanylate cyclase (GC) activity, with the most prominent contribution arising from the GC1 isozyme [7]. In human photoreceptors GCAP2 is probably involved in biochemical processes other than phototransduction [8], although its role in mouse phototransduction has been demonstrated [9].

GCAP1, the main regulator of GC1, is a 23 kDa protein belonging to the EF-hand superfamily [10] that ensures rapid detection of Ca^{2+} oscillations in the submicromolar range with a nanomolar affinity for Ca^{2+} [11]. When Ca^{2+} concentration drops because of phototransduction activation, Ca^{2+} is replaced by Mg^{2+}, which can bind in the same metal binding loops of motifs EF2, EF3 and EF4 (Fig. 1a) [12–14]. This mechanism allows GCAP1 to switch between different signaling states, namely Ca^{2+}-bound (GC1-inhibitor) and Mg^{2+}-bound (GC1-activator), regulated by specific allosteric mechanisms involving the protein, the metal cations and the myristoyl group bound at its N-terminal [13, 15]. The conformation adopted by Mg^{2+}-GCAP1 stimulates the synthesis of cGMP by GC1, thus permitting rapid restoration of dark-adapted cell conditions by reopening of the CNG channels [12, 16]. The Ca^{2+}–Mg^{2+} exchange results in relatively minor conformational changes for GCAP1 [13, 15] (Fig. 1a), which are nevertheless sufficient to trigger the GC1 inhibitor-to-activator transition over the narrow physiological range of Ca^{2+} variation in the photoreceptor outer segment.

GCAP1 has been associated with autosomal dominant cone (COD) or cone-rod dystrophies (CORD) [17–31], a class of severe inherited retinal dystrophies (IRD) characterized by central vision loss, impaired color vision, and photophobia, due to photoreceptor degeneration [32]. Indeed, more than twenty point-mutations in the gene encoding for GCAP1 (*GUCA1A*) have been found to be linked to COD or CORD. Recently, some of us identified a missense mutation in *GUCA1A* responsible for a particularly severe form of CORD. At the protein level, the mutation substitutes a glutamate residue in position 111 with a valine [24]. E111 is the twelfth residue of the Ca^{2+}-binding loop of the EF3 motif and it is directly responsible for Ca^{2+}-coordination by providing two negatively charged oxygen atoms from the carboxyl group (Fig. 1b); this bidentate ligation is fundamental to ensure the correct pentagonal bipyramidal geometry required for coordination of Ca^{2+}-ions by seven oxygen atoms. The hydrophobic sidechain of V111, on the other hand, leads to a structural distortion of the EF3 loop, which becomes unable to coordinate Ca^{2+}-ions (Fig. 1b), thus resulting in an 80-fold lower apparent affinity for Ca^{2+} [24].

COD and CORD remain incurable diseases, and the nature of their transmission — often dominant — makes gene therapy-based approaches particularly challenging. Alternative approaches, for example based on protein delivery, are therefore needed to mitigate the effects of the mutations and re-establish the physiological functionality of the signaling cascade. In this work, we explored the possibility of using direct or liposome-mediated administration of recombinant human GCAP1 to modulate the phototransduction cascade in mouse rods. Our rationale in comparing these two approaches was that free protein could offer high intraocular mobility and acute action, while liposomes delayed but prolonged release. We initially used a model eukaryotic cell culture for protein delivery experiments, and then increased the complexity with in vivo and ex vivo experiments aimed at assessing the biodistribution of proteins in mouse retinas. Imaging experiments were complemented by functional ones, in which acute changes in flash responses were monitored while incubating the retinas ex vivo. The administration of the free and liposome-encapsulated protein was compared in each case. Our findings reveal that direct and liposome-mediated protein delivery are powerful complementary tools for targeting signaling cascades in retinal neurons and could be particularly important for the treatment of autosomal dominant genetic diseases.

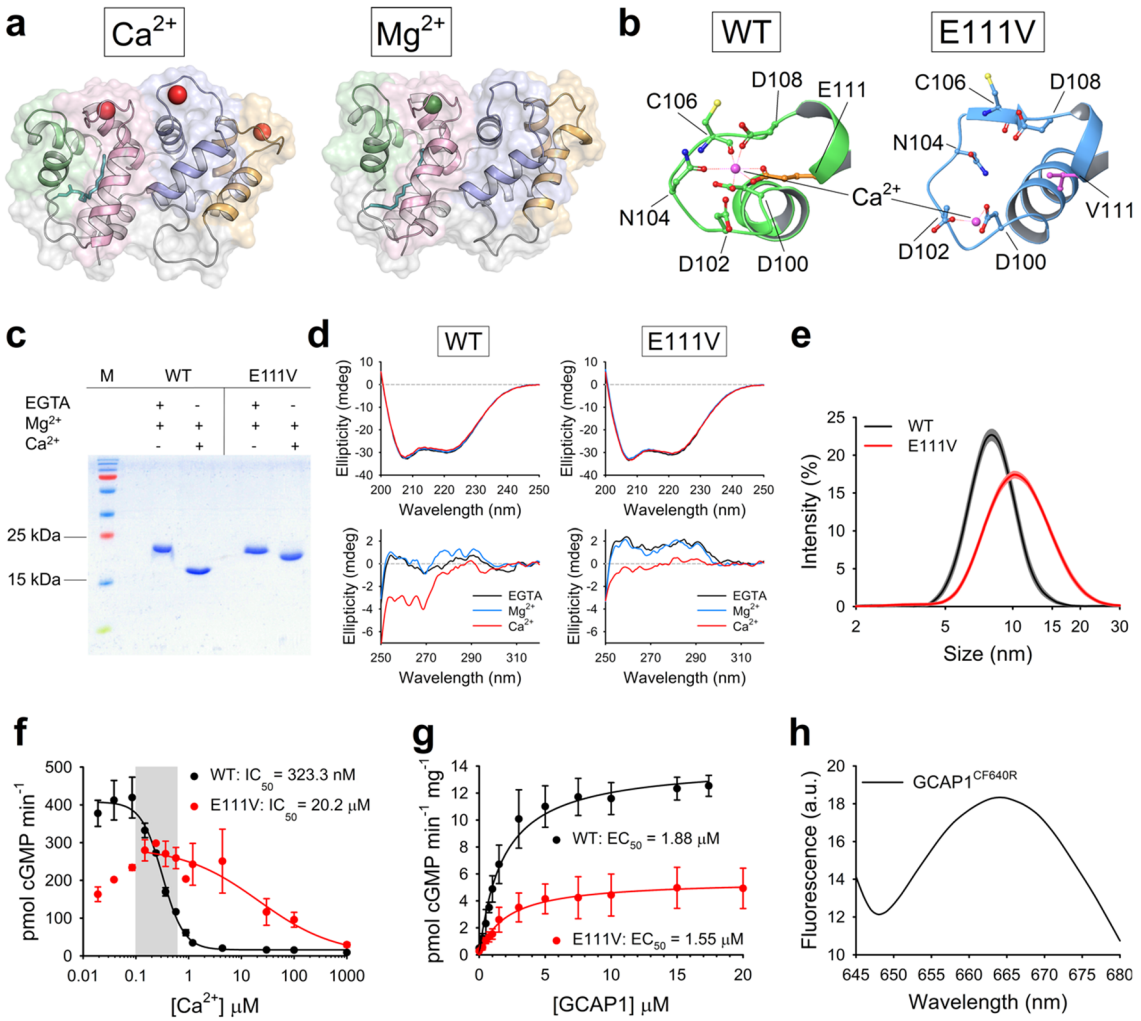

Fig. 1 Biochemical and biophysical characterization of GCAP1 variants. **a** Three-dimensional structure of E111V-GCAP1 in its Ca^{2+}-loaded (left) and Mg^{2+}-bound (right) state after 200 ns Molecular Dynamics (MD) simulations (trajectories are from Ref [24]). Protein structure is represented as cartoons with EF1, EF2, EF3 and EF4 colored in green, pink, blue and orange, respectively; the myristoyl moiety is shown as teal sticks, Ca^{2+} and Mg^{2+} ions are depicted as red and green spheres, respectively. **b** Detail of the Ca^{2+}-binding loop of EF3 in WT-GCAP1 (left) and E111V-GCAP1 (right) after 200 ns MD simulations. Protein structure is shown as cartoons colored in green for WT-GCAP1 and blue for E111V-GCAP1; the sidechains of Ca^{2+}-coordinating residues are labelled and are represented as sticks with O atoms in red, N atoms in blue, S atoms in yellow and C atoms in the same color as cartoons; the C atoms of E111 and V111 residues are colored in orange and magenta, respectively. Ca^{2+}-ions are represented as pink spheres and labelled, zero-order bonds with Ca^{2+}-coordinating residues are shown as dashed red lines; the seventh O atom required for Ca^{2+}-coordination is provided by a water molecule (not shown). **c** 15% SDS-PAGE of ~ 30 µM WT-GCAP1 and E111V-GCAP1 in the presence of 1 mM EGTA + 1.1 mM Mg^{2+} and 1 mM Mg^{2+} + 1 mM Ca^{2+}. **d** Representative far UV (upper panels) and near UV (lower panels) CD spectra of WT-GCAP1 (left panels) and E111V-GCAP1 (right panels) recorded at 25 °C in PBS pH 7.4. Protein concentration for far and near UV was 10 and 33 µM, respectively. Far UV CD spectra were registered in the presence of 300 µM EGTA (black) and after serial additions of 1 mM Mg^{2+} (blue) and 600 µM Ca^{2+} (red), thus resulting in 300 µM free Ca^{2+}. Near UV CD spectra were registered in the presence of 500 µM EGTA and after serial additions of 1 mM Mg^{2+} and 1 mM Ca^{2+} (500 µM free). **e** Hydrodynamic diameter estimation by Dynamic Light Scattering of ~ 40 µM WT-GCAP1 (black) and E111V-GCAP1 (red) at 25 °C in the presence of 1 mM Ca^{2+}; standard errors are shown in grey and orange, respectively. **f** GC1 enzymatic activity as a function of Ca^{2+} concentration (< 19 nM to 1 mM) upon regulation by 5 µM WT-GCAP1 (black) or E111V-GCAP1 (red); cGMP synthesis was half maximal (IC_{50}) at (323.3 ± 15.1) nM and (20.2 ± 7.6) µM with Hill coefficients of 2.16 and 0.99, respectively. The Ca^{2+}-concentration range in photoreceptor cells is represented by the grey box. Data are presented as average ± standard deviation of 3 technical replicates. **g** GC1 activity as a function of WT-GCAP1 (black) and E111V-GCAP1 (red) concentration (0–20 µM range); cGMP synthesis was half maximal (EC_{50}) at (1.88 ± 0.15) µM and (1.55 ± 0.24) µM, respectively. Data are presented as average ± standard deviation of 3 technical replicates after normalization on the amount of GC1 present in cell pellets. **h** Fluorescence emission spectrum of 5 µM $GCAP1^{CF640R}$ upon excitation at 639 nm

Results

Perturbed Ca^{2+}-sensing properties of E111V-GCAP1 lead to constitutive activation of GC1

The purity and functionality of recombinantly expressed GCAP1 variants were verified by a combination of biophysical and biochemical techniques, to exclude potential effects of protein delivery treatments due to impurities or structural/functional defects. Ca^{2+}-sensor proteins, including GCAP1, are known to modify their electrophoretic mobility in SDS-PAGE experiments under denaturing conditions [11], depending on their Ca^{2+}-loading state. Indeed, Ca^{2+}-free proteins appear as single bands at their theoretical molecular weight, whereas their Ca^{2+}-bound forms exhibit an electrophoretic shift to smaller apparent molecular weight proportional to their apparent Ca^{2+}-affinity. Such peculiar behavior exhibited by many other Ca^{2+}-sensor proteins can be attributed to the fact that Ca^{2+}-ions significantly stabilize the structure of the protein and are retained even under denaturing conditions, resulting in a protein that is not fully unfolded, even in the presence of sodium dodecyl sulfate. This makes electrophoretic migration dependent on factors other than just the mass of the protein in the Ca^{2+}-bound form, such as Ca^{2+}-affinity, because the higher the affinity, the greater the probability of partial structure retention. We exploited this peculiar feature to assess both the purity of protein samples and the capability of wild type (WT)-GCAP1 and E111V-GCAP1 to function as Ca^{2+}-sensors (Fig. 1c). In the absence of Ca^{2+}, both purified GCAP1 variants showed a single band around their theoretical molecular weight (23 kDa), which shifted to ~ 17 kDa in the case of WT-GCAP1 and to ~ 20 kDa in the case of E111V-GCAP1 upon Ca^{2+}-binding, thus implying a substantial reduction in Ca^{2+}-affinity for the pathological variant, confirming previous results from some of us [24].

The structural response of GCAP1 variants to ion binding was monitored by circular dichroism (CD) spectroscopy, which allows monitoring changes in protein secondary and tertiary structure in solution at protein concentrations (~ 10 to 40 μM) that mimic physiological ones (~ 3 to 4 μM, Fig. 1d). Both variants exhibited a far ultraviolet (UV) (200–250 nm) CD spectrum compatible with an all α-helix protein, with minima at 208 and 222 nm (Fig. 1d, top panels) and negligible variations in shape and intensity upon ion binding. This behavior was partly in contrast to that previously shown [24], most likely attributable to the different buffer and temperature (PBS pH 7.4 and 25 °C vs 20 mM Tris, 150 KCl, 1 mM DTT, pH 7.5 and 37 °C). Concerning the tertiary structure (near UV CD spectrum, 250–320 nm), both variants displayed a significant rearrangement of aromatic residues upon Ca^{2+}-binding in PBS pH 7.4 at 25 °C (Fig. 1d, bottom panels), indicative of a change in protein tertiary structure. Mg^{2+}-binding instead resulted in a minor conformational change, which was more pronounced in the case of WT-GCAP1. These results were substantially in line with the spectra recorded by some of us at 37 °C, with minor differences attributable to the different buffer and temperature [24], which was found to affect also the hydrodynamic diameter of GCAP1 variants (Fig. 1e). As assessed by dynamic light scattering (DLS), both WT-GCAP1 and E111V-GCAP1 in PBS, pH 7.4 displayed a significantly larger hydrodynamic diameter ((8.68 ± 1.07) nm and (11.08 ± 0.07) nm, respectively), compared to their counterparts in 20 mM Tris, 150 mM KCl, 1 mM DTT, pH 7.5 buffer ((6.47 ± 0.03) nm and (6.08 ± 0.04) nm, respectively) [24], a difference ascribable to the absence of the reducing agent and of a centrifugation step in this study, which nevertheless did not trigger any aggregation process (results not shown). The slightly different experimental conditions of the present and the previous study [24] lead to the same conclusions that the E111V substitution significantly impairs the Ca^{2+}-sensitivity of GCAP1 with minor structural repercussions.

The enzymatic activity of the GCAP1-GC1 complex and its Ca^{2+}-dependence creates a tight interconnection between Ca^{2+} and cGMP levels, which is crucial for both light adaptation and photoreceptor viability. Regulation of the GC1 enzymatic activity by GCAP1 variants was assessed both in terms of Ca^{2+} sensitivity and dependence on the level of protein regulator by measuring, respectively, the Ca^{2+} concentration at which GC1 activation is half-maximal (IC_{50}) and the concentration of GCAP1 at which the synthesis of cGMP is half-maximal (EC_{50}). The activation profile of GC1 by WT-GCAP1 exhibited an IC_{50} of (323.3 ± 15.1) nM (Fig. 1f), thus falling in the physiological intracellular Ca^{2+}-range (< 100 to 600 nM) [5]. On the other hand, the pathological variant E111V significantly dysregulated the activity of GC1, with an IC_{50} value ((20.2 ± 7.6) μM, p-value < 0.05) ~ 63-fold higher than that of the WT, indicative of constitutive cGMP synthesis under physiological Ca^{2+} levels. Nevertheless, both variants displayed comparable EC_{50} values ((1.88 ± 0.14) μM for WT-GCAP1 and (1.55 ± 0.23) μM for E111V-GCAP1 (p-value > 0.1), Fig. 1g), suggesting a similar affinity for the target enzyme, in line with previous results from some of us [24].

Liposome-mediated GCAP1 delivery to HEK293 cells

To assess the potential of liposome (LP)-mediated delivery of GCAP1 in biological systems of increasing complexity (in cyto, ex vivo, and in vivo) and investigate its biodistribution by minimizing the contribution of tissue auto-fluorescence

(see Methods), the far-red fluorescent dye CF640R was conjugated to the primary amines of solvent-exposed Lys residues of GCAP1 (namely, either of K8, K23, K24, K46, K87, K97, K142 or K162, Movie S1) to obtain the GCAP1^{CF640R} complex. SDS-PAGE confirmed the purity of protein samples and the success of the conjugation reaction (Fig. S1a). The effective removal of the unconjugated dye (Fig. S1b) and the number of CF640R molecules bound to each GCAP1 protein were then assessed by absorption spectroscopy (degree of labelling = 1.96, see Methods). Finally, the emission fluorescence spectrum of GCAP1^{CF640R} (Fig. 1h) upon excitation at 639 nm was recorded before imaging experiments to verify the compatibility of the conjugated dye with our optical setups. The unconjugated dye (CF640R), GCAP1^{CF640R}, WT-GCAP1 and E111V-GCAP1 were then encapsulated in LPs with a lipid composition corresponding to that of rod outer segment membranes (see Methods for details).

The suitability of LP as carriers of small molecules and proteins was assessed by evaluating the size and monodispersion of the liposome suspensions loaded with different molecules. Regardless of the type of encapsulated molecule, nanoparticle tracking analysis (NTA) measured a LP diameter between (149.1 ± 3.0) nm and (168.7 ± 0.7) nm (Fig. S2a–c, Table S1), with minor differences in both size and concentration (Table S1) up to 180 days (Fig. S2d–f), suggesting that the LP suspension is stable over time. Finally, effective encapsulation of fluorescent molecules was also visually confirmed by the display of point-like fluorescence emission when LPs were filled with unconjugated CF640R and immobilized in agarose gel (Fig. S2g).

The capability of LPs to deliver recombinant GCAP1^{CF640R} was assessed on two different HEK293 stable cell lines. The first was transfected with pIRES plasmid encoding for eGFP and GC1 under the same promoter, characterized by a cytosolic green fluorescence (from now on cGFP); the second was transfected with pcDNA3.1 encoding for the eGFP-GC1 fusion protein, thus showing membrane green fluorescence (mGFP).

To address the potential direct membrane uptake of free-CF640R due to its small size (~832 Da) we monitored the cGFP cell line for 6 h (Movie S2) and visualized the mGFP cell line for 6 h and 24 h after incubation with free-CF640R (Fig. 2a). The absence of intracellular red fluorescence in both cell lines after 6 h and 24 h suggested that free-CF640R is per se unable to penetrate cell membranes.

Indeed, a diffused red fluorescence signal was observed only in the extracellular milieu, in the same time frames (Fig. 2a). This signal is likely attributable to the presence

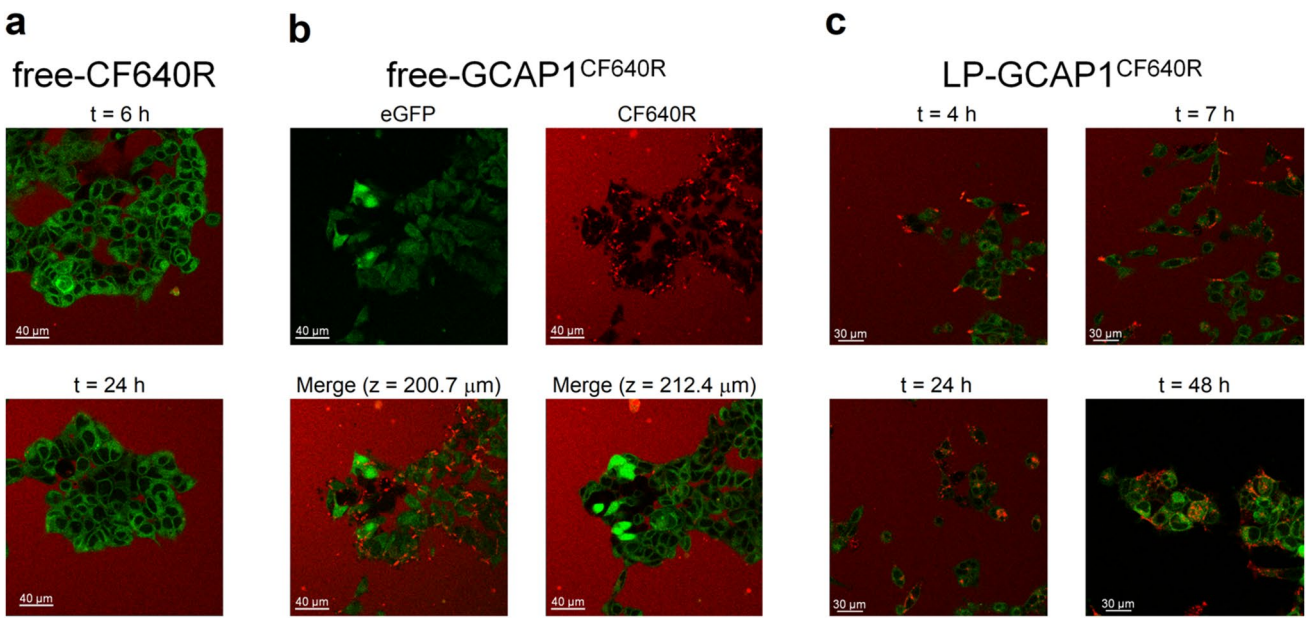

Fig. 2 Live imaging of HEK293 cells incubated with free-CF640R, free-GCAP1^{CF640R} and GCAP1-encapsulating liposomes. **a** representative images at a fixed z-plane of the mGFP cell line incubated with 100 µl of 140 µM free-CF640R after 6 h (top) and 24 h (bottom); **b** representative images of the mGFP cell line after 24 h incubation with 100 µl of 104 µM free-GCAP1^{CF640R}, top panels show eGFP (left) and CF640R (right) fluorescence, bottom panels show the merged fluorescence at z = 200.7 µm (left) and z = 212.4 µm (right). **c** Live-cell imaging at the same z-plane of the mGFP cell line after 4 h, 7 h, 24 h, and 48 h incubation with 100 µl of 4.3 nM LP-GCAP-1^{CF640R} (containing the same number of GCAP1^{CF640R} molecules in the aqueous core as compared to the free protein solution case). After 24 h the cell medium was replaced with FluoroBrite DMEM to avoid interference from phenol red, which gave rise to the red background fluorescence present in all but bottom right panel

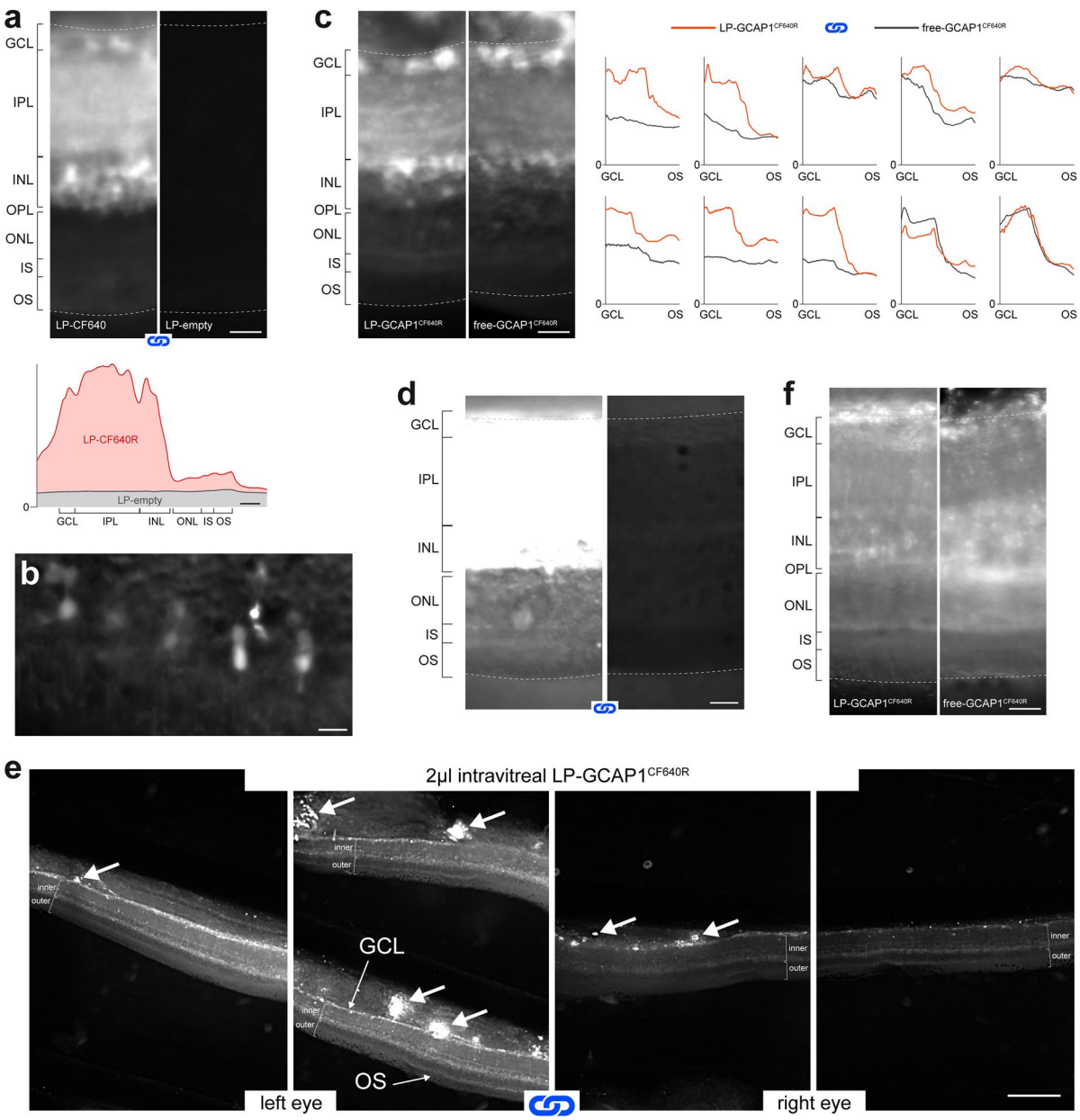

Fig. 3 Biodistribution of free GCAP1 and liposome-encapsulated GCAP1 in living mouse retinas following ex vivo incubation and in vivo intravitreal injections. **a** Distribution of fluorescence in 250 µm thick live slices obtained from a pair of retinas incubated ex vivo with 20 µl of 3.9 nM LP-CF640R and 5.1 nM LP-empty, respectively: the same image acquisition and display parameters were used (blue chain links symbol). Plot shows the average fluorescence along the vertical axis of the same images. Scale bars 25 µm. **b** Fluorescent cones in a slice from a retina incubated with 20 µl of 3.9 nM LP-CF640R. Scale bar 10 µm. **c** Distribution of fluorescence after ex vivo incubation with 20 µl of 88.4 µM free-GCAP-1^{CF640R} and 4.3 nM LP-GCAP1^{CF640R} (containing the same number of GCAP1^{CF640R} molecules in the aqueous core as compared to the free protein solution case). In the example images the focal plane was intentionally set to display zones rich with stained neuronal somata. Scale bar 25 µm. Plots show radial fluorescence profiles across retina pairs in each experiment; blue chain links: the same acquisition parameters were used in each retina pair. **d** Distribution of fluorescence after ex vivo incubation with 88.4 µM free-GCAP1^{CF640R} and PBS. The white point of the images was adjusted to enhance the outer retina: same acquisition and display parameters. **e** Low magnification examples of retinal slices from the eyes of a mouse, both intravitreally injected with identical aliquots of 4.3 nM LP-GCAP-1^{CF640R}: the same acquisition and display parameters were used (blue chain links). Thick white arrows: zones of accumulation of fluorescence in the vitreous humor near the inner limiting membrane. Inner: GCL + IPL + INL; outer: ONL + IS + OS. Scale bar 250 µm. **f** Examples of the distribution of fluorescence in retina slices after intravitreal injection with 2 µl of 88.4 µM free-GCAP1^{CF640R} and 4.3 nM LP-GCAP1^{CF640R} (containing the same number of GCAP1^{CF640R} molecules in the aqueous core as compared to the free protein solution case). Scale bar 25 µm. In all images of this figure the focal plane lies deep in the slice. In all experiments retinal layer boundaries were identified as shown in Fig. S9

of phenol red in the medium, as in real time imaging no medium replacement was performed.

Similar experiments performed with fluorescently labelled GCAP1 (GCAP1^{CF640R}), showed punctuated fluorescence spots which tended to accumulate on the surface of mGFP cells after 6 h (Movie S3; punctuated red fluorescence is attributable to the interaction of GCAP1^{CF640R} with other molecules in the cell medium or with cell membrane, at odds with the diffused phenol red fluorescence). The intracellular space was not reached by the labelled protein even after 24 h (Fig. 2b, top panels). Further analysis at specific z-plane values (bottom panels in Fig. 2b) clearly confirmed that the accumulation of fluorescence attributed to GCAP1^{CF640R} is limited to the cell membrane, as no signal was detected at the intracellular space. To confirm this finding, we repeated the same experiment with cGFP cells, which would allow the detection of overlapped green and red fluorescence signals in case of GCAP1^{CF640R} entering the intracellular milieu. Indeed, this was not observed in 6 h (Movie S4). To dampen the contribution of diffused red fluorescence from the extracellular milieu, we replaced the cell medium with FluoroBrite DMEM, which does not contain phenol. The same results were confirmed (Fig. S3), indicating that GCAP1^{CF640R} did not enter HEK293 cells in the observed timeframe.

As both cGFP and mGFP cell lines exhibited the same impermeability to free-CF640R and free-GCAP1^{CF640R}, the capability of liposomes to deliver GCAP1^{CF640R} was tested only on the mGFP cell line. Live-cell imaging showed that 4 h after incubation (Fig. 2c, Movie S5), a punctuated red fluorescence, compatible with that emitted by LP-GCAP-1^{CF640R}, was accumulating on the cell surface. At t = 7 h, the same punctuated red fluorescence was distinctly detected in the cytosol, suggesting whole liposome internalization by the cells. Only after 24 h the fluorescence pattern started to change. A more diffused red signal initially appeared at around 24 h, indicative of the release of GCAP1^{CF640R} from LPs. The observation of red and green colocalized fluorescence was more apparent at t = 48 h, indicative of a more unhindered diffusion of GCAP1^{CF640R} in the cytosol (Fig. 2c and Fig. S4), although the persistence of the punctuated pattern suggests the residual presence of internalized liposomes. Finally, 48 h after incubation with LP-GCAP1^{CF640R} the cell medium was replaced with FluoroBrite DMEM to improve the signal-to-noise ratio; while a more diffused colocalization of red and green fluorescence attributed to the intracellular release of GCAP1^{CF640R} was more clearly observed (Fig. S4d), residual quantal fluorescence was present.

Retinal distribution in live tissue of GCAP1^{CF640R} and LP-GCAP1^{CF640R} following ex vivo incubation and intravitreal injection

Ex vivo incubations

To move to a higher level of biological complexity, we first assessed LP-mediated delivery of molecules by ex vivo incubation of isolated retinas. The rationale here was to eliminate variability related to in vivo transport across tissues, focusing solely on intraretinal mechanisms. Far red fluorescence was chosen because in preliminary tests we found that the extremely low tissue autofluorescence in this band greatly improved signal-to-noise ratio. Retina pairs (n = 3) were incubated in parallel with LP-CF640R and LP-empty suspensions for 2 h at 37 °C. After incubation, these live retinas were rinsed with fresh medium and immediately viewed with a widefield fluorescent microscope either as wholemounts or 250 µm thick slices, with the two treatment partners placed adjacent in the dish. In all cases the LP-CF640R-treated retina showed fluorescence much above the control one. Unexpectedly, fluorescence was unevenly distributed across the thickness of the retina, being much stronger in the inner layers (Fig. 3a). Nonetheless, even the outer retina showed a significant signal. Control slices had a flat autofluorescence profile, at the level of the chamber background. Interestingly, in the LP-CF640R-treated retinas sparse cell bodies in the ganglion cell (GCL) and inner nuclear layer (INL) could be clearly distinguished. In the outer retina cones were also occasionally stained (Fig. 3b), albeit much more rarely than the aforementioned neurons. These data suggest enrichment of LPs in the inner retina, although it remained unclear whether they were internalized as intact nanovesicles or their fluorescent cargo released in the cell.

To determine whether LP encapsulation affects the tissue access of large molecules, we incubated retina pairs (n = 10) with free-GCAP1^{CF640R} protein solution or LP-GCAP1^{CF640R} suspension for 3.5 h at 37 °C, followed by slicing and imaging with identical parameters. The average fluorescence of the inner retina (GCL + IPL + INL) and photoreceptors (ONL + IS + OS) was measured to quantitatively assess tissue distribution. As we had observed qualitatively for LP-CF640R, fluorescence in the inner retina was 168% (SD 50%) of that in photoreceptors following incubation with LP-GCAP1^{CF640R} ($p < 0.01$, n = 10; paired Wilcoxon test) and 160% (SD 55%) of photoreceptors with free-GCAP1^{CF640R} ($p < 0.001$, n = 12) (Fig. 3c). Furthermore, treatment with LP-encapsulated protein led to significantly higher fluorescence compared to free protein in both the inner retina (150% of free protein, SD 52%; p-value < 0.05, n = 10) and photoreceptors (127% of free protein, SD 21%; p-value < 0.01, n = 10) (Fig. 3c). In

the GCL and INL distinctly stained neuronal somata were observed after both types of incubations (Fig. 3c, images). It must be noted that, even in the photoreceptor layer, signal from retinas incubated with the free protein was well above the level of tissue autofluorescence. This was confirmed by comparing incubation with free protein and PBS for 3.5 h at 37 °C (n = 2; 152% and 162%) (Fig. 3d). Interestingly, the peculiar distribution of both free and LP-encapsulated GCAP1^{CF640R} was also observed in retinas incubated with free CF640R fluorophore (Fig. S5a). We ruled out a significant contribution of the unbound fluorophore to the distribution observed with free-GCAP1^{CF640R}, as its concentration in our samples was estimated to be < 1% of the labelled protein (see Methods). Furthermore, during the preparation of LP-GCAP1^{CF640R} (encapsulation and subsequent washing) any residual unbound fluorophore would have fallen to even lower levels. Thus, had such traces of unconjugated fluorophore played a significant role in our experiments, we would have obtained results opposite to those shown in Fig. 3c (i.e. a higher signal in free-GCAP1^{CF640R}-incubated retinas).

Intravitreal injections

We went on to examine retinal delivery in vivo by injecting intravitreally free-GCAP1^{CF640R} solution and LP-GCAP-1^{CF640R} suspension in the two eyes. After 20–24 h in darkness the animals were sacrificed, their retinas isolated, sliced 250 µm thick and viewed as live tissue with a widefield fluorescence microscope. Both retinas were imaged in the same session using identical acquisition parameters. We found that most injections led to some degree of retinal fluorescence (LP-GCAP1^{CF640R}: n = 9 out of 12; free-GCAP1^{CF640R}: n = 6 out of 11). Notably, while fluorescence was similar in different slices from the same retina, it varied greatly from eye to eye despite our utmost care in performing reproducible injections. This intrinsic variability was confirmed in a subset of animals in which both eyes were injected with identical solutions (n = 3 pairs; Fig. 3e). Importantly, it hindered our ability to detect any significant differences in the delivery of LP-GCAP1^{CF640R} and free-GCAP1^{CF640R} to the retina (n = 9 pairs). It is worth noting that residues of vitreous humor still adhering to the inner limiting membrane were often strongly fluorescent (Fig. 3e thick white arrows). Similarly to ex vivo incubated retinas, average fluorescence was quantified in the inner retina and photoreceptors. In those retinas displaying fluorescence after intravitreal injection, the inner layers were significantly brighter than the photoreceptors, both in the case of LP-GCAP1^{CF640R} (120% of photoreceptors, SD 22%; p-value < 0.05, n = 8) and free-GCAP1^{CF640R} (121% of photoreceptors, SD 19%; p-value < 0.05, n = 6) (Fig. 3f). This mimicked what was observed in ex vivo incubations. However, following intravitreal injections individual cell bodies did not stand out (Fig. 3f): perhaps in these experiments there was sufficient time for uniform uptake by all neurons. Diffuse retinal fluorescence could be similarly observed after intravitreal injection of free CF640R fluorophore (Fig. S5b). In summary, we found that intravitreal injections are a viable, albeit rather inconsistent, means of delivery of free or encapsulated proteins to the retina.

Immunofluorescence reveals different timing for free and LP-encapsulated GCAP1 internalization

Despite some discrepancies in the observed biodistribution, partly due to its inherent variability, the ex vivo incubation and intravitreal injection experiments suggested that fluorescently labeled GCAP1 can be internalized by all retinal layers. To study biodistribution by a complementary methodology, we repeated the ex vivo incubation experiments using a variant of GCAP1 with a His-tag at the C-terminus (GCAP1^{His}), which allowed direct detection by immunofluorescence. Incubation was performed for both free GCAP1^{His} and LP-GCAP1^{His} using the same protocol used for CF640R-conjugated counterparts, at three different time intervals, namely, (i) 30 min; (ii) 4 h and 30 min; and (iii) 24 h (Fig. 4).

Incubation of the untreated tissue with a primary antibody against the His-tag resulted in an almost nonexistent background signal (Fig. 4a), which allowed high-resolution detection of the internalized GCAP1^{His} protein by immunofluorescence.

A substantially different time-course of protein internalization was observed when comparing the free and LP-encapsulated protein. Delivered free-GCAP1^{His} (Fig. 4b) was observed in both inner and outer retina even after 30 min, with a detectable signal at the photoreceptor layer (yellow arrow). Fluorescence increased with incubation time, resulting in a clear accumulation of protein in the photoreceptor layer, with specific signals both in the IS and OS layers. Interestingly, 24 h after incubation the delivered protein was clearly visible in the somata of several ganglion cells (yellow arrow in Fig. 4b, right panel), but a much stronger signal was present in the photoreceptor layer even within individual cones (Fig. 5a, yellow arrows and insets). In the case of LP-GCAP1^{His}, the intra-retinal signal became detectable only after a few hours, and at t = 4 h 30 min a speckled signal was observed at the level of the OPL (yellow arrow in Fig. 4c), suggesting that LPs were only partially internalized and did not release their content. However, at t = 24 h, a strong signal was observed in both inner and outer retina and individual ganglion cell somata became visible, along with the photoreceptor layer region. At this time, an overlap of the signal with that of the individual cones was observed (Fig. 5b and inset), indicating that the liposomes released their contents within the individual photoreceptors.

In summary, our comparative experiments show a substantially different timing of retinal internalization for free

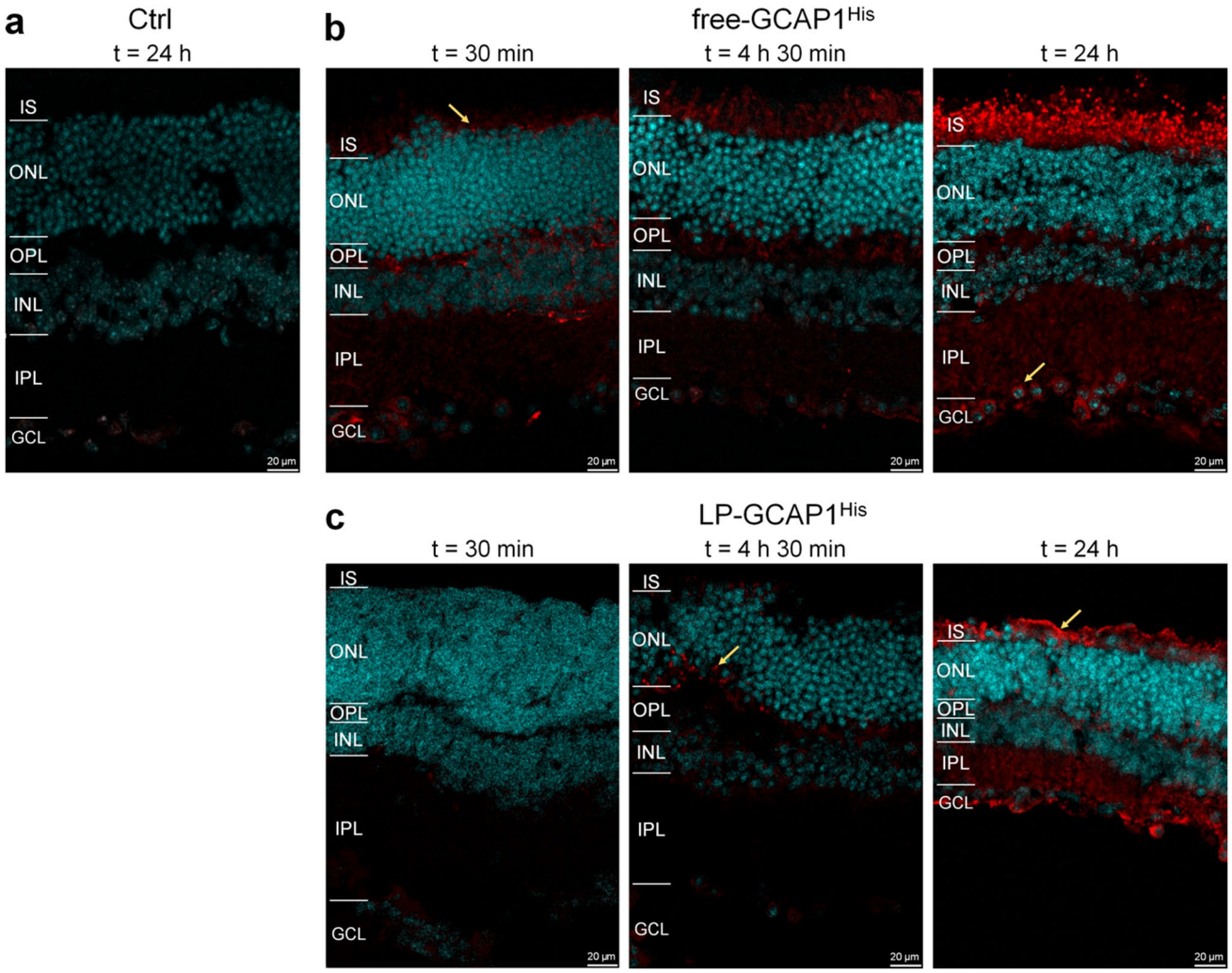

Fig. 4 Distribution of delivered recombinant GCAP1^{His} in mouse retinas following ex vivo incubation as detected by immunofluorescence. Representative central plane of Z-stack of retinal cryosections after **a** 24 h of incubation with 180 µl PBS; **b** 30 min, 4 h 30 min and 24 h incubation with 180 µl of 99.6 µM free-GCAP1^{His}. **c** 30 min, 4 h 30 min and 24 h incubation with 180 µl of 4.5 nM LP-GCAP1^{His} (containing the same number of GCAP1^{His} molecules in the aqueous core as compared to the free protein solution case). Sections were stained with an anti-His antibody (red) and DAPI (light blue). The same image acquisition and display parameters were used in all samples

and LP-encapsulated GCAP1, which reflects in a slightly different biodistribution of exogenous protein across the retinal layers, as shown by the alternative presence of more diffused and speckled signals (Fig. S6).

Delivery of E111V-GCAP1 induces a CORD-like phenotype in WT mouse retinas

If a protein such as GCAP1 was able to gain access to retinal neurons in sufficient concentration, it could potentially be used to modulate biochemical processes [33]. As a proof of concept, we tested the functional effects on photoreceptors of E111V-GCAP1, known to be associated with CORD [24]. Ex vivo ERG recordings were made in a novel purpose-built chamber (see Methods), which enabled prolonged incubation of retinas with relatively high concentrations of expensive test substances (i.e., using tiny overall amounts). ERG recordings were made at 35 °C (except when stated otherwise) under pharmacological blockade of synaptic transmission to ON-bipolars (40 µM AP4) [34]. Except in one case, we did not remove the slow glial component with $BaCl_2$ in order to avoid any direct or secondary effects on photoreceptor physiology, which could affect unpredictably liposome and/or protein uptake [35]. The above conditions were associated to stable recordings of scotopic flash responses for over 4 h. Two parameters were extracted: (*i*) light sensitivity measured by the flash intensity required to obtain a 50% response (i_{50}); (*ii*) time to peak of the 50% response (TTP@

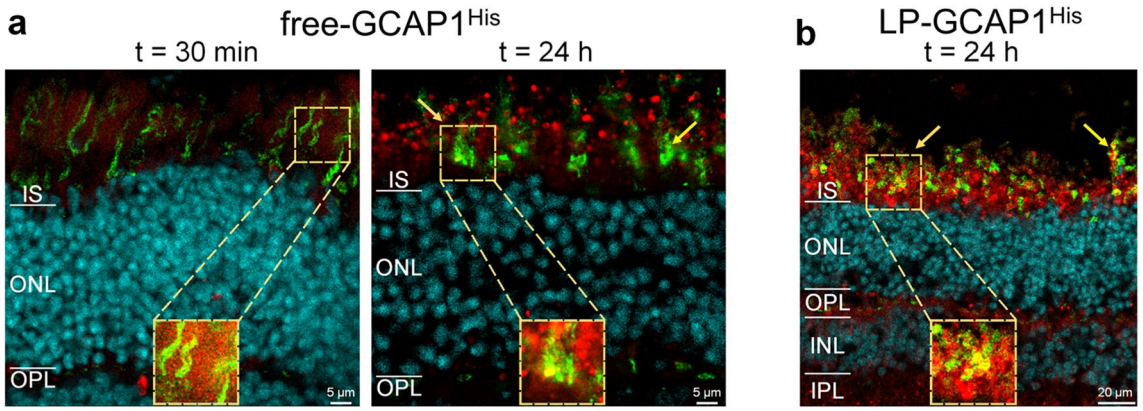

Fig. 5 Cellular distribution of delivered recombinant GCAP1^{His} in mouse retinas following ex vivo incubation as detected by immunofluorescence. Representative central plane of Z-stack of cryosections of retinas after **a** 30 min and 24 h incubation with 180 µl of 99.6 µM free-GCAP1^{His}; or **b** 24 h incubation with 180 µl of 4.5 nM LP-GCAP1^{His} (containing the same number of GCAP1^{His} molecules in the aqueous core as compared to the free protein solution case). Sections stained with an anti-His antibody (red), DAPI (light blue) and Peanut Agglutinin (PNA, green). The same image acquisition and display parameters were used in all samples. Insets show individual cones with the red point of the images adjusted to enhance the signal for GCAP1^{His}. Note the signal overlap from the two channels, resulting in yellow pixels, indicating intracellular location.

i_{50}) (Fig. S7). These were normalized to their pre-treatment levels and processed to remove any trends also present in the control retina, leaving us with (ideally) the net effect of treatment (see Methods).

We first compared the incubation with WT-GCAP1 to PBS (n = 14 animals; Fig. 6a). Over three hours of incubation no significant and systematic effects were detected either on sensitivity or kinetics (Fig. 6a). However, the incubation with free-E111V-GCAP1 slowed response kinetics when compared to PBS (n = 14; Fig. 6b), an effect highly significant already from the first minutes after delivery through the entire three hours of incubation ($p < 0.01$). We confirmed this surprising result by comparing the same concentration of free-E111V-GCAP1 and free-WT-GCAP1, again observing a highly significant slowing of kinetics at most time points (n = 8; Fig. 6c), which indicated that the effect is attributable solely to the E111V point mutation. It should be noted that, even 30 min after incubation, the exogenous protein was observed to be internalized by the retina and was detected in the photoreceptor layer (Fig. 4b). The phenotypic effect was therefore induced very rapidly.

We then went on to examine the effect of LP encapsulation. According to immunofluorescence data (Fig. 4c), LPs were observed after 4 h 30 min incubation in the OPL and, to a lesser extent also in the photoreceptor layer, although the fluorescence pattern suggested that their cargo may not have been released during this time. When LPs-empty were compared to PBS no significant effects were detected (n = 13; Fig. 6d), suggesting that LPs by themselves do not perturb phototransduction. Interestingly, LP-E111V-GCAP1 compared to PBS did not replicate the effects seen with the free mutant protein (n = 9; Fig. 6e). Based on our experience with LPs holding fluorescent molecules we hypothesized that LPs might be scavenged by the filter paper supporting the retina in the chamber. To exclude this possibility, we modified our approach to hold the retinas in place during the recordings thereby dispensing with the filter paper. Furthermore, to promote LP fusion/internalization in cells we raised the incubation temperature to 37°C. Despite these efforts no significant effects were detected over the course of 3 h (n = 21; Fig. 6f). We also compared the incubation of free-E111V-GCAP1 with LP-E111V-GCAP1 (n = 7) and, given previous results, we were not surprised to find a significant slowing of kinetics throughout incubation (Fig. 6g). A weakly significant increase in light sensitivity, not seen in previous comparisons was observed. Furthermore, we confirmed that free-E111V-GCAP1 slow response kinetics also when 50 µM $BaCl_2$ is present in the bath solution (n = 5; Fig. 6h; Fig. S8), although these incubations were terminated after about 1 h. Taking into account the results from immunofluorescence, we reasoned that while LPs might be rapidly internalized, their contents could be released over much longer time scales, also in line with previous findings [36, 37]. To begin examining this hypothesis we exploited recent advances by some of us in long duration ex vivo ERG [38] and succeeded to prolong incubations of LP-encapsulated protein to 18 h. When comparing LP-E111V-GCAP1 to PBS, we detected a significant slowing of the response kinetics only in the final few time bins (n = 18; Fig. 6i), thus approaching 24 h after incubation. This result is fully in line with immunofluorescence experiments, which clearly show that efficient release of the protein following LP encapsulation takes longer than delivery of the free protein, particularly to reach adequate levels in the photoreceptor layer and

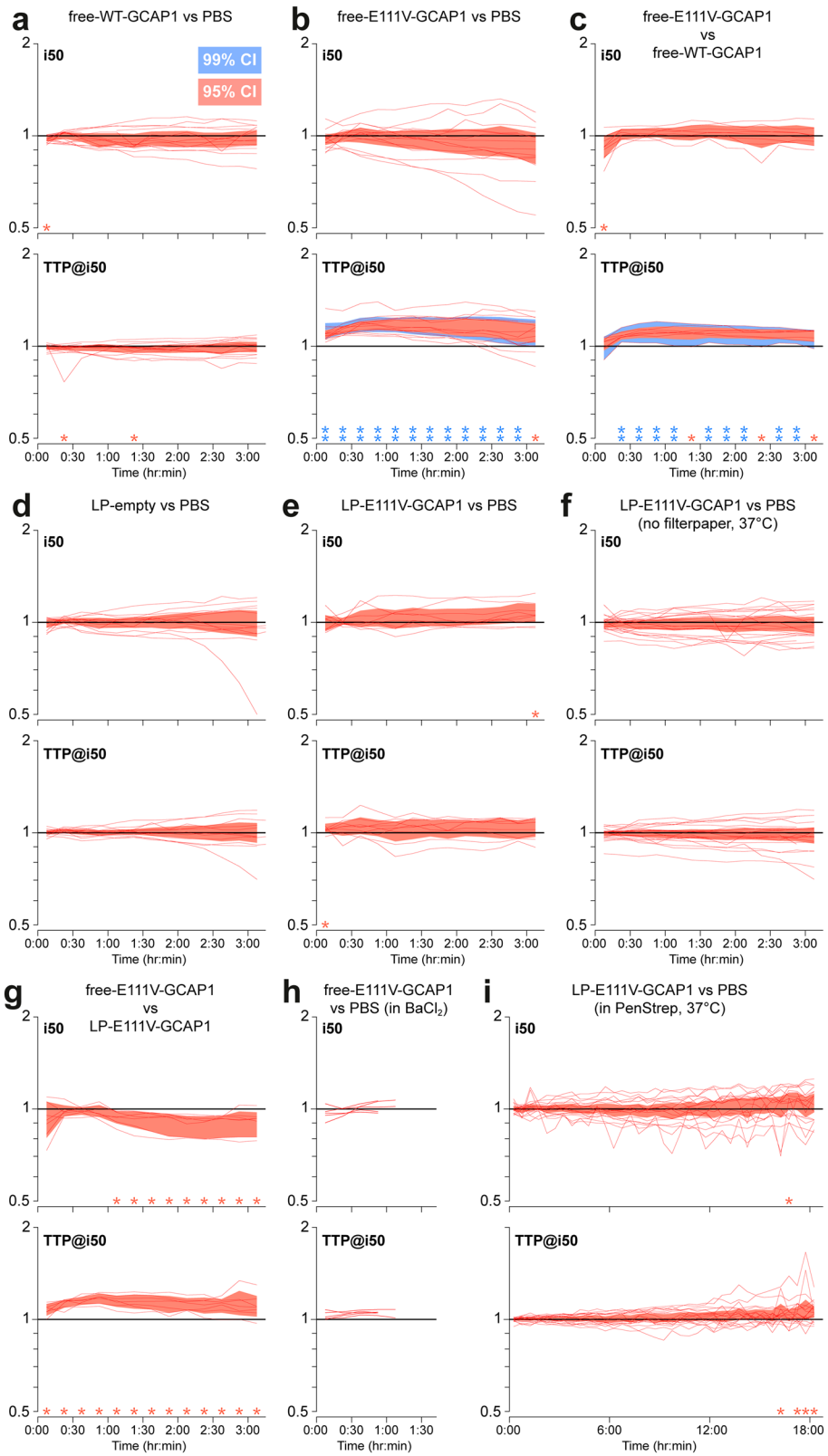

Fig. 6 Functional effects on isolated retinas of incubation with free or LP-encapsulated recombinant GCAP1. The ex vivo ERGs of retina pairs were obtained in control conditions (Time < 0) and during parallel incubation with test and reference solutions for up to 3 h or 18 h. Changes in light sensitivity (i_{50}) and response kinetics (TTP@i_{50}) were monitored by normalizing for pre-treatment control and reference solution. **a**–**i** Red lines represent individual experiments, each involving both retinas from an animal. Red (blue) shaded areas cover the 95% (99%) confidence interval. Loci above unity indicate a decrease in sensitivity or a slowing in kinetics. Red stars: p-value < 0.05; double blue stars: p-value < 0.01

specifically in the outer segment. While our recordings are the state of the art in terms of duration, only future technical developments will allow to monitor the effects of slow drug release by liposomes over several days.

Discussion

In recent years, delivery of proteins and peptides to the eye have emerged as promising avenues for the treatment of a variety of ocular diseases [39], although significant physiological and anatomical challenges remain [40], especially when the goal is to modify biochemical processes occurring in the outer retina. In particular, to assist the development of effective therapies, basic knowledge is needed on whether and how different proteins/peptides move across the ocular compartments [41]. Our investigation represents a proof of concept that protein delivery to the retina may indeed be an effective strategy to modify the phototransduction cascade, which could be relevant to the treatment of IRDs.

Our experiments were based on the delivery of recombinant GCAP1 variants, whose in vitro characterization showed that the CORD-associated E111V-GCAP1 mutant constitutively activates GC1 as a consequence of its impaired Ca^{2+} sensing, although without altering its affinity (EC_{50}) for the target. Furthermore, the Ca^{2+} sensitivity of the GC1-GCAP1 system reconstituted in vitro was perfectly in line with the intracellular Ca^{2+} changes that occur in photoreceptors during phototransduction activation, thus demonstrating the functionality of recombinant proteins.

The simplest system used in this work for testing the potential of protein delivery was eukaryotic cell lines. Experiments with two different lines of HEK293 cells expressing GC1 clearly showed that fluorescently labelled GCAP1 ($GCAP1^{CF640R}$) tended to accumulate near the membrane but did not cross it. In contrast, 4 h after incubation, the same LP-encapsulated protein (LP-$GCAP1^{CF640R}$) started to enter the cell and was clearly observed in the cytoplasm 24 and even 48 h later. Considering that HEK293 cells were impermeable to the unconjugated dye and that $GCAP1^{CF640R}$ failed to cross cell membrane in a 24 h timeframe, this suggests that liposomes are indeed required to transport GCAP1 inside these cells.

Experiments performed with mouse retinas unveiled a completely different scenario. Both free and LP-encapsulated $GCAP1^{CF640R}$ were found to enter retinal neurons in the short time span of our ex vivo incubations (4.5 h), although with different timing and efficacy, as highlighted by immunofluorescence experiments. This also occurred 20–24 h after intravitreal injection, although in this case the fluorescence was locally uniform in the tissue. This could be due to the relatively short time following injection and lower effective protein concentration in intravitreal injections, as immunofluorescence suggests that only prolonged incubation results in cell-specific distribution. The mechanisms underlying retinal biodistribution of endogenous proteins deserves dedicated attention in future studies, using ad hoc model systems, such as organotypic retina cultures that permit high-resolution monitoring of the biodistribution of delivered protein. Besides the efficient delivery to the outer retina, in both ex vivo incubation and intravitreal experiments we detected particularly efficient delivery to the inner retina, suggesting that ocular diseases affecting retinal ganglion cells may be particularly well suited to protein therapy approaches relying on the delivery of recombinant proteins, either with or without the use of LPs as vectors. On the other hand, our functional studies demonstrate that the extent of delivery of exogenous GCAP1 into the photoreceptor outer segments is sufficient to modify the phototransduction cascade.

Taken together, the contrasting data obtained when comparing cell cultures and mouse retinas suggest that cell membrane composition plays an important role in determining the fate of free extracellular GCAP1. The lipid composition of HEK293 membranes [42] significantly differs from that of photoreceptors, which is known to change during retinal development [43] as well as between cone- or rod-dominant retinas [44], and in pathological conditions [43, 45]. Moreover, photoreceptors possess a host of complex and only partially understood molecular mechanisms of communication with the extracellular environment, including a high rate of synaptic membrane turnover due to synaptic vesicles exo/endocytosis [46] or disk membrane and nutrient recycling [47]. Thus, the complexity of retinal lipid composition and metabolism could partly explain the differences observed in the two cell types. Indeed, liposomes with a lipid composition that mimics the photoreceptor membrane are apparently able to enter both HEK293 and retinal neurons, although the process takes at least 24 h in the former, while being significantly faster in the latter. Our results indicate that exogenous GCAP1 can, in the absence of lipid carrier, cross retinal cell membranes and quickly achieve a detectable concentration in both the inner and outer layers, at odds with HEK293 cells, where no protein internalization was observed even after 24 h. While we did not anticipate such behavior, comparably challenging feats by exogenously applied proteins are not unprecedented. Indeed, even without clarifying the inherent mechanisms, several studies performed both in murine and human systems have previously shown that nerve growth factors can potentially cross several barriers in the visual system upon topical (eyedrops) [48] or intravitreal administration [49], leading to tangible clinical outcomes. Nevertheless, the mechanism by which intracellular distribution of exogenous GCAP1 can be observed across different neuronal layers remains currently unknown. Perhaps the protein distribution among photoreceptors is somehow related to the recently discovered nanotube-like connections [50, 51] that allow the exchange of intracellular material [52] including whole proteins. As for the inner-to-outer retina protein exchange, it could be mediated by glial transcytosis operated by Müller cells [53]. These cells generate the

inner limiting membrane between the vitreous humor and the retina and span the whole retina longitudinally. Uptake of proteins and liposomes by Müller cells following intravitreal injections could therefore explain the broad retina biodistribution observed in our in vivo experiments. These hypotheses, which have tremendous implications for protein targeted therapy of retinal diseases, need further investigation.

In a comprehensive set of electrophysiological experiments, we found that free human E111V-GCAP1 rapidly induces a significant slowing of the photoresponse. Crucially, the WT protein did not evoke this effect, thereby pointing to a key role of the E111V point mutation. On the broader level this finding provides strong independent confirmation that free GCAP1 is taken up by retinal neurons and reaches the OS, where the phototransduction machinery is located. On the specific level of phototransduction it is striking, considering the compensating effect played by GCAP2 in murine photoreceptors [9, 33, 54]. In stark contrast, when the mutant protein was delivered encapsulated in LPs no such effects on kinetics were observed in 3 h long incubations and recordings. However, electrophysiological recordings performed over a longer time scale of up to 18 h, suggest that liposomes could be initially internalized intact, while only over longer times scales release their cargo, in line with immunofluorescence in this study and previous results [36, 37]. In fact, the latter property can be considered a major benefit in terms of sustained release and drug pharmacokinetics, be it the case of encapsulated small molecules [55] or, as shown by our study, recombinant proteins.

In a previous study we incubated mouse retinas for 2 h at 37 °C with LPs containing either the protein recoverin (homologous to GCAP1) or an antibody against the same protein [56]. In that case, we observed a significant difference in saturating response kinetics between the two treatments. The lipid composition of those liposomes was somewhat different (phosphatidylcholine/cholesterol at various molar ratios) than that used in the present work. Also different was the electrophysiological recording technique (loose seal patch clamp from single rods), which did not require a pharmacological blockade of synaptic transmission nor involve the presence of a slow glial ERG response component. Aside from these relatively minor differences, a key factor could be the relative ability of the different proteins to perturb phototransduction. If, as postulated above, liposomes slowly release their cargo once inside the photoreceptors, a functional effect after 2–3 h may only be detectable when delivering a strongly impacting protein. Recoverin antibody could, in principle, possess such an effect, considering the crucial role of the recoverin-mediated Ca^{2+}-feedback on rhodopsin kinase in accelerating the shutoff [57]. In contrast, in the present study the recombinant GCAP1 mutant had to outcompete the endogenous WT protein and the compensating effect of GCAP2, which would overall occur when a sufficiently high amount of exogenous GCAP1 has reached the photoreceptor outer segment.

An unexpected finding of this study is that intravitreal injections in mice show extreme trial-to-trial variability in the translocation of delivered molecules to the retina. It must be noted that while mouse eyeballs are approximately tenfold smaller than human eyeballs (3 mm vs 24 mm diameter), their respective vitreous chambers exhibit a 1000-fold difference in volume (4.4 µl vs 4.3 ml [58]). This, together with the high intraocular pressure after injection, renders the entire procedure much more difficult to reproduce in mice than in human, for which several approved eye therapies are administered via intravitreal injections, and could result in lower effective concentration of delivered protein. We intentionally injected an excess volume of 2 µl to ensure that, despite some inevitable backward reflux through the injection hole, a significant amount of test solution always remained in the eye (utmost care was taken in this respect). We would thus tend to attribute a significant part of the variability observed to complex flow dynamics or inhomogeneities in the vitreous. Whatever the mechanism, studies employing intravitreal injections in mice should carefully consider whether variability in their observed therapeutic effects may have the same origin. Clearly, demonstrating significant effects of a drug candidate (or conversely excluding any medically relevant effects) may require a high number of test subjects.

Our study shows that direct and liposome-mediated protein delivery, while acting over different time scales, are powerful complementary tools for targeting signaling cascades in neuronal cells and could be particularly important for the treatment of retinal diseases. While genome editing represents the most promising therapeutic approach for the treatment of IRDs [59], a number of issues remain to be addressed, such as the risk of integrating viral DNA into the host genome increasing the likelihood of oncogenesis in the case of widely used viral vectors. Moreover, persistent expression of the editing machinery could give rise to antiviral immune responses in the long term; finally, the viral vectors currently in use pose severe limitations for the delivery of large genes needed for most gene therapies [60]. On the one hand, our study shows that LPs may represent ideal nonviral vectors for even large gene delivery, or they could be used to deliver ribonucleoproteins by eliciting a low immunogenic response, thus representing a promising strategy for genome editing in the eye. On the other hand, we have clearly shown that administration of recombinant proteins that mimic endogenous ones can induce a specific phenotype in retinal neurons, and this could have therapeutic relevance, especially in cases of autosomal dominant transmission, where a pool of mutated protein is responsible for the disease-phenotype. In the specific case of COD-CORD associated with missense mutations in GCAP1, a possible

mutation-independent approach to therapy could be the delivery of WT-GCAP1 to overcome the effect of the mutant protein. In the case of the E111V variant, this strategy relies on two robust findings. First, WT- and E111V-GCAP1 show very similar apparent affinity for GC1 (EC_{50}), therefore could stoichiometrically compete for the same GC1 target. Second, our previous findings [33] demonstrated in vitro that the prolonged administration of exogenous GCAP1 could attenuate the pathological phenotype by: (i) shifting the IC_{50} towards physiological values, with an increase in cooperativity of cGMP synthesis; (ii) reshaping the photoresponses towards a wild-type like kinetics; (iii) re-establish a wild-type-like homeostasis of second messengers (Ca^{2+} and cGMP) in dark-adapted cells. The proof-of-concept study presented here has therefore high therapeutic potential.

The implications of our findings could extend to a broader scale. Indeed, the GPCR-mediated molecular machinery building up the phototransduction cascade is shared by other signal transduction processes, including chemotaxis, neurotransmission, cell communication, activation of olfaction and taste, and many others [61]. Understanding the mechanisms that influence this signaling cascade and achieving its controlled modulation is critical for drug discovery, since about one-third of all drugs on the market target members of class A GPCRs [2]. More specifically, considering that GCAP1 is the major regulator of GC1 in human photoreceptors and that an increasing number of point mutations in its gene are associated with autosomal dominant COD or CORD, the development of novel biological therapies targeting this protein may help to restore the dysregulation of second messenger homeostasis in IRDs, ultimately slowing or blocking cell death.

Materials and methods

Materials

Tris(hydroxymethyl)aminomethane (Tris), Guanidine-HCl, NaCl, KCl, $CaCl_2$, $MgCl_2$, DTT, EGTA, β-mercaptoethanol, NH_4HCO_3, 4-(2-hydroxyethyl)-1-piperazineethanesulfonic acid) (HEPES), Ames' medium, ethanolamine, phosphatidylethanolamine, phosphatidylcholine, phosphatidylserine, cholesterol, acrylamide, Coomassie blue, cGMP, polyethyleneimine, sucrose, OCT, NH_4Cl, citric acid, Triton X-100, Tween 20, Bovine Serum Albumin, chloramphenicol, cOmplete EDTA-free Protease Inhibitor Cocktail, paraformaldehyde, ketamine, xylazine, atropine, hydrocortisone and $BaCl_2$ were purchased from Merck (Darmstadt, Germany).

DMEM, OptiMEM, penicillin, streptomycin, 2-(4-amidinophenyl)-1H-indole-6-carboxamidine (DAPI), Phosphate Saline Buffer (PBS), Fetal Bovine Serum (FBS), HBSS, glutamine, Normal Goat Serum, Normal Donkey Serum were purchased from ThermoFisher Scientific (Waltham, MA, USA).

Cloning, expression, and purification of GCAP1 variants

Human myristoylated WT-GCAP1 was expressed in *E. coli* BL21 (DE3) after co-transformation with pBB131 containing the cDNA of *S. cerevisiae* N-myristoyl transferase (yNMT) [62]. The cDNA for E111V variant was obtained by PCR using QuikChange II Site-Directed Mutagenesis kit (Agilent, Milan, Italy) as described in Ref [24], while the cDNA for His-tagged WT-GCAP1 ($GCAP1^{His}$) was purchased from Genscript. Both variants were expressed and purified following the same protocol as for the WT [33], briefly consisting of: (*i*) denaturation of inclusion bodies with 6 M Guanidine-HCl; (*ii*) refolding by dialysis against 20 mM Tris–HCl pH 7.5, 150 mM NaCl, 7.2 mM β-mercaptoethanol, and a combination of (*iii*) Size Exclusion Chromatography (SEC, HiPrep 26/60 Sephacryl S-200 HR, GE Healthcare, Chicago, IL, USA) and (*iv*) Anionic Exchange Chromatography (AEC, HiPrep Q HP 16/10, GE Healthcare, Chicago, IL, USA). The purity of GCAP1 variants was assessed by 15% acrylamide SDS-PAGE, samples were either exchanged against PBS, aliquoted and frozen with liquid nitrogen, or exchanged against NH_4HCO_3, aliquoted and lyophilized. Protein samples were finally stored at -80 °C.

The three-dimensional structure of human GCAP1 was obtained by homology modeling using the structure of Ca^{2+}-loaded chicken GCAP1 [63] following the procedure illustrated in Ref [18]. In silico mutagenesis of E111V variant was obtained according to the protocol detailed in Ref [24]. The structures presented in Fig. 1a and b were extracted from the last frame of 200 ns Molecular Dynamics simulations from Ref [24], whose settings and protocols for energy minimization, equilibration and production phases were elucidated in Refs [13, 15].

Electrophoretic mobility shift assay

WT-GCAP1 and E111V-GCAP1 were dissolved in 20 mM Tris–HCl pH 7.5, 150 mM KCl, 1 mM DTT at a concentration of 30 µM, incubated for 5 min at 25 °C with either 1 mM EGTA + 1.1 mM Mg^{2+} or 1 mM Mg^{2+} + 1 mM Ca^{2+}, boiled, and run for 50 min at 200 V on a 15% acrylamide gel under denaturing conditions. Finally, protein bands were visualized by Coomassie blue staining.

Circular dichroism (CD) spectroscopy

The effects of ion binding and of the E111V substitution on the secondary and tertiary structure of GCAP1 were

evaluated by CD spectroscopy using a J-710 spectropolarimeter (Jasco, Cremella, Italy) thermostated by a Peltier-type cell holder. Lyophilized proteins were dissolved in PBS pH 7.4 buffer at a concentration of 35 and 10 µM for near UV and far UV spectra, respectively. Five accumulations of each spectrum were recorded at 25 °C in the absence of ions (500 µM EGTA for near UV, 300 µM for far UV) and after serial additions of 1 mM Mg^{2+} and Ca^{2+} (1 mM for near UV, 600 µM for far UV, leading to a free Ca^{2+} concentration of 500 and 300 µM, respectively). All spectra were subtracted with that of the buffer, near UV spectra were also zeroed by subtracting the average ellipticity between 310 and 320 nm, where no signal was expected.

Dynamic light scattering (DLS)

The hydrodynamic diameter of Ca^{2+}-loaded WT-GCAP1 and E111V-GCAP1 was estimated by DLS using a Zetasizer Nano-S (Malvern Instruments, Malvern, UK). Proteins were dissolved in PBS pH 7.4 at 42 µM concentration and filtered with a Whatman Anotop 10 filter (20 nm cutoff, GE Healthcare, Chicago, IL, USA) before starting the measurements. Samples were equilibrated for 2 min at 25 °C and for each variant at least 100 measurements were collected, each consisting of 13 runs.

Guanylate cyclase activity assay

GC1 enzymatic activity as a function of Ca^{2+} and GCAP1 concentration was measured after reconstituting WT-GCAP1 and E111V-GCAP1 with cell membranes of mGFP-GC1 cells (see below) previously extracted by lysis (10 mM HEPES pH 7.4, Protease Inhibitor Cocktail 1×, 1 mM DTT buffer) and 20 min centrifugation at 18,000×g, as previously described [30, 64, 65]. Cell membranes were resuspended in 50 mM HEPES pH 7.4, 50 mM KCl, 20 mM NaCl, 1 mM DTT and incubated with 5 µM GCAP1 variants at increasing [Ca^{2+}] (< 19 nM to 1 mM, controlled by Ca^{2+}-EGTA buffer solutions [66]) to estimate the Ca^{2+} concentration at which cGMP synthesis by GC1 was half-maximal (IC_{50}). To estimate the GCAP1 concentration at which GC1 activation was half-maximal (EC_{50}), cell membranes were reconstituted with increasing amounts of each GCAP1 variant (0–20 µM) at low Ca^{2+} (< 19 nM). Reported IC_{50} and EC_{50} values are represented as average ± standard deviation of 3 technical replicates. The statistical significance of the differences in IC_{50} and EC_{50} between WT-GCAP1 and E111V-GCAP1 was evaluated by means of two-tailed t tests (p value = 0.05).

Conjugation of CF640R-N-hydroxysuccinimide (NHS) ester with WT-GCAP1

Far-red fluorescent dye CF640R (Biotium, Fremont, CA, USA) was conjugated via NHS to WT-GCAP1 primary amines (Lys residues, Movie S1) according to the manufacturer protocol. Briefly, GCAP1 was diluted in PBS pH 7.4 and 1 mM DTT to a final concentration of 76 µM in a final volume of 900 µl; then the solution was added with 100 µl sodium bicarbonate 1 M pH 8.3 and 2 CF640R-NHS aliquots previously resuspended in 50 µl total DMSO. The mixture was then wrapped in aluminum and incubated in rotation at RT for 1 h. Unconjugated dye was removed by washing 4 times the protein solution (see Fig. S1b for representative spectra of the 4 flowthrough) with PBS pH 7.4 for 10 min at 4400 × g and 4 °C using an Amicon Ultra-4 concentrator with 3 kDa cutoff (Merck Millipore, Burlington, MA, USA). The degree of labelling (DOL = 1.96) was calculated as the ratio between the concentration of dye in the protein solution measured based on the absorbance at 642 nm ($\varepsilon = 105.000\ cm^{-1}\ M^{-1}$), and the concentration of protein calculated by considering the dilution factor and the retention of Amicon concentrators (95%, according to manufacturer instructions). The concentration of free-CF640R in the protein solution was calculated by measuring the absorbance at 642 nm of wash 4, which was < 1% with respect to protein concentration in all conjugation experiments. Unconjugated dye was blocked with 50 µl ethanolamine 1 M.

Fluorescence spectroscopy

The emission fluorescence spectrum of 2 µM $GCAP1^{CF640R}$ (645–680 nm) dissolved in PBS pH 7.4 was collected at 25 °C on a FP-750 spectrofluorometer (Jasco, Cremella, Italy) after excitation at 639 nm; the spectrum reported in Fig. 1h is an average of 3 accumulations after subtraction of the emission spectrum of the buffer in the same range.

Liposome preparation

LPs were prepared by hydrating a thin lipid film of the same composition as photoreceptors rod outer segment membranes [67] (phosphatidylethanolamine, phosphatidylcholine, phosphatidylserine, and cholesterol at a molar ratio of 40:40:15:5) previously mixed in chloroform and dried in a speed-vac concentrator. Four mg of lipid film were hydrated with 1 ml PBS pH 7.4, vortexed for 30 min at room temperature, sonicated for 15 min in a water bath on ice and extruded 20 times through a 200 nm polycarbonate filter (Whatman, Maidstone, UK). The encapsulation of CF640R, WT-GCAP1, E111V-GCAP1, $GCAP1^{His}$, or $GCAP1^{CF640R}$ in LPs was achieved by dissolving the molecule to be loaded in PBS before lipid film hydration. Unencapsulated

molecules were removed by washing at least 4 times the LPs suspensions with PBS pH 7.4 for 20 min at 4 °C and 5000×g using an Amicon Ultra-4 concentrator with 100 kDa cutoff (Merck Millipore, Burlington, MA, USA). The degree of encapsulation was calculated by subtracting from the total mass of the molecule to be encapsulated that present in the flow-through and was found to be higher than 75% in all LP preparations. The efficient separation of non-encapsulated proteins was assessed by measuring protein concentration of the flowthrough of the 4 washing steps, similarly to what was done for CF640R. The concentration of non-encapsulated protein in LP suspensions was estimated from the concentration of protein in the last washing step and was found to be < 7% of the encapsulated protein.

Nanoparticle tracking analysis (NTA)

The concentration and size of LP suspensions were measured at 25 °C by means of NTA on a NanoSight (Malvern Instruments, Malvern, UK) by recording 3 videos of 1 min each at 25 fps by setting 20 µl/min flow rate; camera level and detection threshold were automatically optimized for each measurement to maximize the signal-to-noise ratio. LP size reported in Fig. S2 and LP concentration reported in Table S1 represent the average ± standard error of 3 technical replicates.

Fluorescence imaging of gel-immobilized liposomes

Stock suspensions of LPs, either filled with free-CF640R or empty, were diluted 1:400 v/v in 0.5% low gelling temperature agarose in Ames' medium at 37 °C. A thin film was polymerized over a pure agarose meniscus in a Petri dish and covered with Ames' medium. 3D image stacks were acquired with a 63x/0.9NA water immersion objective and a CCD camera (DFC350 FX, Leica Microsystems, Milan, Italy) in an upright widefield fluorescence microscope (DM LFSA, Leica Microsystems, Milan, Italy) using a Cy5 filterset (49,006; Chroma, Olching, Germany). Stacks were deconvolved and max projected along the z-axis using Fiji/ImageJ as detailed in Ref [68].

Generation of cGFP-GC1 and mGFP-GC1 stable HEK293 cell lines

HEK293 cells were cultured in DMEM medium supplemented with fetal bovine serum (10%, v/v), penicillin (100 units/ml) and streptomycin (100 µg/ml) at 37 °C in humidified atmosphere with 5% CO_2. Cells (6.25×10^5) were seeded in 6-well plates in DMEM medium and grown overnight; the next day cell medium was replaced with OptiMEM reduced serum medium and cells were transfected using polyethyleneimine (PEI) as transfection reagent and 2 different vectors to obtain eGFP-expressing stable cell lines: (*i*) pIRES encoding for eGFP and human GC1 under the same promoter, thus resulting in a cytosolic fluorescence (cGFP), and (*ii*) pcDNA3.1 + N-eGFP encoding for GC1-eGFP fusion protein for localizing fluorescence on the membrane (mGFP). DNA (2.5 µg) was mixed dropwise to 10 µl PEI solution at a concentration of 1 µg/µl (DNA:PEI ratio of 1:5 w/w), added dropwise to 500 µl of pre-warmed OptiMEM, mixed and incubated 30 min at room temperature to allow DNA-PEI polyplex formation. Polyplexes were finally added dropwise to each well and the plate was incubated overnight at 37 °C and 5% CO_2. The next day, OptiMEM medium was replaced with DMEM and 48 h after transfection eGFP positive cells were selected using geneticin (500 µg/ml).

Live-cell imaging

Cells (8×10^4) were seeded in 4-well chambers (Ibidi, Graefelfing, Germany) in DMEM medium; two days later the medium was replaced with OptiMEM reduced serum medium, then cells were incubated with 100 µl LP suspension per well (containing each ~ 0.4 mg lipid) and monitored in live-cell imaging. Experiments with fluorescently labelled $GCAP1^{CF640R}$ were performed taking care of incubating the cells with the same nominal concentration of protein encapsulated in the LP aqueous core.

Live-cell imaging was performed using TCS-SP5 Inverted Confocal Microscope (Leica Microsystems, Milan, Italy) equipped with temperature and CO_2 controller and motorized stage that provides precise and automated acquisition of multiple fields of view. Images were collected simultaneously on different points of the sample immediately after cell-LP incubation and at 30 min interval for 24 h or 48 h total acquisition time. Images were captured after 488 nm and 633 nm laser excitation with a 40× objective (1.2 NA oil immersion) and further analyzed by Imaris 9.8 software (Oxford Instruments, Abingdon-on-Thames, UK). The fluorescence intensity profiles of mGFP and LP-$GCAP1^{CF640R}$ reported in Fig. S4 were collected along the line across the cell shown in the insets using ImageJ.

Fluorescence microscopy of mouse retinas following ex vivo incubation

All animal experiments made use of adult C57Bl/6 J mice of both sexes. These were reared at around 22 °C in small groups with the addition of environmental enrichment items, a 12 h day/12 h night cycle, ad libitum food and water. As in previous studies by our group, and in accordance with authorized protocols, dark adapted mice were deeply anesthetized with ketamine (80 mg/kg) + xylazine (5 mg/kg) and their retinas extracted through a corneal incision in room temperature Ames' medium under dim red light. This

approach avoided even brief exposure of the tissue to anoxic conditions, which could affect protein and/or liposome uptake. Animals were then immediately sacrificed with an overdose of anesthetic. After removing the vitreous each retina was placed, freely floating, in a plastic well containing incubation solution (1–2 ml depending on the experiment), and the wells inserted in an airtight box with a water layer at the bottom and a 95%O_2/5%CO_2 atmosphere. Incubation solutions consisted in the test suspension/solution diluted in Ames' medium, taking care of reaching virtually the same final concentration for each suspension. The box was left floating in a water bath at 37 °C. After the prescribed time the retinas were returned to room temperature Ames' medium, made to adhere to black filter paper (AABP02500; Merck, Burlington, MA, USA) with gentle suction and, optionally, sliced at 250 µm thickness with a manual tissue chopper. Image stacks were acquired as described for the imaging of gel-immobilized LPs, with 4x/0.1NA air, 20x/0.5NA and 40x/0.8NA water immersion objectives. Excitation was provided by an Hg lamp preheated to achieve stable output. Stacks were lightly deconvolved (Richardson-Lucy algorithm, 10 iterations) and a single image obtained by averaging along the z-axis a few adjacent slices of the stack, in all cases chosen well below the cut surface. The borders of retinal layers were identified by imaging the same tissue volume in the near IR (Fig. S9). Cones were identified based on their characteristic location and morphology, leveraging our experience with their intracellular staining. Identical acquisition parameters were used when comparing retinas treated with different incubation solutions.

Immunofluorescence experiments with mouse retinas following ex vivo incubation

Mice were anesthetized with isoflurane, euthanized via cervical dislocation and their retinas extracted through a corneal incision in room temperature DMEM medium supplemented with FBS (25%, v/v), HBSS (25% v/v), glutamine (1% v/v), penicillin (100 units/ml) and streptomycin (100 µg/ml). After 30 min incubation at 37 °C and 5% CO_2, tissues were incubated with 180 µl PBS, 180 µl of 100 µM free-GCAP1^{His} or 180 µl of 4.5 nM LP-GCAP1^{His} (containing the same number of GCAP1^{His} molecules in the aqueous core as compared to the free protein solution case) for 30 min, 4 h 30 min, and 24 h, and finally washed 3 times with PBS.

Retina sections were then fixed for 40 min in 10% formalin in PBS buffer, washed 3 times with PBS, incubated with 10%, 20% and 30% sucrose for 1 h each at RT, and kept overnight at 4 °C. The next day samples were incubated at RT for 1 h with OCT compound: 30% sucrose at a 1:1 ratio and processed for cryo-sectioning at – 14 °C.

Sections (14 µm thickness) were fixed for 5 min with paraformaldehyde, washed 3 times with PBS, incubated with 0.1% Triton X-100 in PBS for 1 h at RT, washed 3 times with PBS, incubated with ammonium chloride for 20 min, and washed 5 times with PBS.

Sections were incubated overnight at RT with mouse anti-His primary antibody (1:1000 dilution, SouthernBiotech, Birmingham, AL, USA) and PNA (1:250 dilution, Molecular Probes, Eugene, OR, USA) in blocking solution (5% Normal Goat Serum, 1% Bovine Serum Albumin, 0.3% Triton X-100 in PBS). The following day samples were washed 3 times with PBS and incubated with an Alexa Fluor 647-conjugated goat anti-mouse secondary antibody (1:1000 dilution, Invitrogen, Waltham, MA, USA). Cell nuclei were stained with a 1:1000 DAPI dilution in PBS; slides were coverslipped with Dako fluorescence mounting medium (Agilent, Milan, Italy). Sections were visualized using TCS-SP5 Inverted Confocal Microscope (Leica Microsystems, Milan, Italy), images were captured after 405 nm and 633 nm laser excitation with a 63× objective (1.2 NA oil immersion) and further analyzed by Imaris 9.8 software (Oxford Instruments, Abingdon-on-Thames, UK).

Intravitreal injections

Mice were first anesthetized with ketamine (80 mg/kg) + xylazine (5 mg/kg), followed by application of eyedrops containing atropine and chloramphenicol (1%) + hydrocortisone (0.5%). Intravitreal injections were made under a stereomicroscope and dim blue light as follows: (*i*) a hole was made in the cornea near the *ora serrata* with the tip of a 31G insulin needle; (*ii*) glass micropipettes with a broken tip, connected to a 25 µl syringe (Hamilton, Reno, NV, USA) via PE tubing filled with mineral oil (330,779; Merck, Burlington, MA, USA), were front loaded with 2 µl of solution; (*iii*) the micropipette was inserted in the hole and the entire volume slowly injected in the vitreous. Mice were returned to their cages and allowed to recover in a paper blanket. After 20–24 h we performed retinal dissection, slicing and imaging as described for ex vivo incubations.

Long duration ex vivo ERG recordings

ERG experiments were made in a custom designed incubation and recording chamber [38]. Retina pairs were isolated as described for ex vivo incubations, made to adhere to white filter paper (SMWP02500; Merck, Burlington, MA, USA) and placed at the bottom of two adjacent plastic wells, containing 2 ml/retina of 40 µM AP4 (0101; Tocris, Milan, Italy) in Ames' medium. Retinas were centered on a hole leading to the anode, while the cathode was in the chamber itself. In some experiments we dispensed with

the filter paper and used instead small transparent cups to immobilize the retinas (Fig. 1b in Ref [38]). Both electrodes were silver chloride wires inserted in an agar bridge. The well assembly was placed on an aluminum platform covered with a layer of water, inside a sealed incubation chamber purged with 95% O_2/5% CO_2. The temperature of the platform was actively controlled with a custom apparatus [69]. Small diameter PTFE tubing, leading from inside the wells to syringes residing outside the chamber, allowed injection and mixing of test solutions (100 µl/retina) into the wells during the recordings with minimal perturbation. Immediately above the wells, attached to the lid of the chamber, a LED (505 nm; ND filters) delivered the same flash sequence every 15 or 30 min: (ph/µm^2|no. of flash repetitions) 3.98|12, 8.27|10, 18.9|8, 50.5|6, 151|6, 510|4, 1660|3. Transretinal potentials were amplified by 5000, filtered in the band DC-100 Hz, digitized at 5 kHz and acquired with pClamp 9 (Molecular Devices, San Jose, CA, USA). Electrophysiological records were analyzed in Axograph X with automated custom scripts. i_{50} was determined by fitting a Hill function to a plot of response amplitudes measured 90–130 ms after the flash (Fig. S7). This range minimized the contribution of the very slow glial response and gave parameter values close to those in $BaCl_2$ [38]. TTP@i_{50} was estimated as the weighted average of the TTPs of the two flash responses straddling i_{50} (10 Hz Gaussian filtered records). Two rounds of normalization were applied to these raw data, as follows. We assumed that the two retinas, being from the same animal, behaved identically except for (*i*) an initial stabilization phase due to slight variations in their isolation and manipulation, and (*ii*) a scaling factor in their steady state light sensitivity due to small differences in their orientation in the recording chamber. We first normalized the two sets of raw values over their respective pre-treatment levels. We then removed any trends common to both retinas by dividing the normalized values of the treated retina by those of the control. We were thus left with a single time series that shows the net effect of the tested drug (Fig. 6, red lines). Treated and control retina positions in the wells were alternated from animal to animal to cancel out any environmental biases. In a limited number of tests (Fig. 6h) $BaCl_2$ was injected in the wells using the syringe system after an initial stabilization period and stirred to obtain a final concentration of 50 µM. In a subset of the experiments, we included HyClone PenStrep (SV30010; Cytiva, Breisgau, Germany) in the incubation medium at 1% vol/vol, which enabled us to prolong our recordings up to 18 h.

Statistics

Statistical analyses were performed with the open-source software JASP 0.16 (jasp-stats.org; RRID:SCR_015823), Kaleidagraph 5 and Excel (Microsoft, Redmond, WA, USA). For ERG recordings visual representation of the population effect of a tested drug (Fig. 6) were given by the confidence interval of the Hodges-Lehmann estimator [38]. Statistical significance was estimated by the following parametric and non-parametric tests as mentioned in the text: two tailed t-test, paired Wilcoxon signed-rank, one sample Wilcoxon signed-rank.

Supplementary Information The online version contains supplementary material available at https://doi.org/10.1007/s00018-023-05022-0.

Acknowledgements The Centro Piattaforme Tecnologiche of the University of Verona is acknowledged for providing access to spectroscopic and imaging platforms. We thank Carmen Longo for helpful discussions.

Author contributions SA and LC performed the ex vivo and in vivo experiments. VM, AB and GDC performed in vitro experiments. AA performed in cyto and live imaging experiments. DD and LC conceived and designed the study and supervised the project. All authors analyzed the data and contributed to design and write the manuscript with the supervision of LC and DD. All authors have read and approved the manuscript.

Funding Open access funding provided by Università degli Studi di Verona within the CRUI-CARE Agreement. This study was supported by a grant from the Velux Stiftung (Project No. 1410), by the following Next Generation EU/Ministry of University and Research projects: *(i) "Tuscany Health Ecosystem (THE)", CUP I53C22000780001, milestones 4.3.2 (spoke 4) and 8.9.1 (spoke 8); (ii) "A multiscale integrated approach to the study of the nervous system in health and disease (MNESYS)", CUP B33C22001060002, PE00000006 missione 4, componente 2, investimento 1.3. The kind support of Retina Italia OdV is gratefully acknowledged.*

Availability of data and materials The datasets generated during and/or analyzed during the current study are available from the corresponding authors on reasonable request. Source data are provided with this paper.

Declarations

Conflict of interest The authors have no relevant financial or non-financial interests to disclose.

Ethics approval and consent to participate This study was performed in line with the principles of the Declaration of Helsinki. Approval for all the animal procedures employed was granted by the Ethics Committee of Universities of Verona and Pisa, and the Italian Ministry of Health (authorization n. 937/2021-PR referred to prot. n. 56DC9.74), in accordance with the Italian (D.lgs.vo 116/92 and D.lgs 26/2014) and EU regulations (Council Directive 86/609/EEC).

Consent for publication Not applicable.

References

1. Deupi X (2014) Relevance of rhodopsin studies for GPCR activation. Biochim Biophys Acta 1837:674–682. https://doi.org/10.1016/j.bbabio.2013.09.002
2. Zhou Q et al (2019) Common activation mechanism of class A GPCRs. Elife. https://doi.org/10.7554/eLife.50279
3. Koch KW, Dell'Orco D (2015) Protein and signaling networks in vertebrate photoreceptor cells. Front Mol Neurosci 8:67. https://doi.org/10.3389/fnmol.2015.00067
4. Korenbrot JI (2012) Speed, sensitivity, and stability of the light response in rod and cone photoreceptors: facts and models. Prog Retin Eye Res 31:442–466. https://doi.org/10.1016/j.preteyeres.2012.05.002
5. Koch KW, Dell'orco D (2013) A calcium-relay mechanism in vertebrate phototransduction. ACS Chem Neurosci 4:909–917. https://doi.org/10.1021/cn400027z
6. Dell'Orco D, Koch KW, Kreutz MR, Naranjo JR, Schwaller B (2019) Editorial: neuronal calcium sensors in health and disease. Front Mol Neurosci 12:278. https://doi.org/10.3389/fnmol.2019.00278
7. Peshenko IV et al (2011) Enzymatic properties and regulation of the native isozymes of retinal membrane guanylyl cyclase (RetGC) from mouse photoreceptors. Biochemistry 50:5590–5600. https://doi.org/10.1021/bi200491b
8. Avesani A, Marino V, Zanzoni S, Koch KW, Dell'Orco D (2021) Molecular properties of human guanylate cyclase-activating protein 2 (GCAP2) and its retinal dystrophy-associated variant G157R. J Biol Chem 296:100619. https://doi.org/10.1016/j.jbc.2021.100619
9. Vinberg F, Peshenko IV, Chen J, Dizhoor AM, Kefalov VJ (2018) Guanylate cyclase-activating protein 2 contributes to phototransduction and light adaptation in mouse cone photoreceptors. J Biol Chem 293:7457–7465. https://doi.org/10.1074/jbc.RA117.001574
10. Heizmann CW (2019) Ca(2+)-binding proteins of the EF-hand superfamily: diagnostic and prognostic biomarkers and novel therapeutic targets. Methods Mol Biol 1929:157–186. https://doi.org/10.1007/978-1-4939-9030-6_11
11. Dell'Orco D, Sulmann S, Linse S, Koch KW (2012) Dynamics of conformational Ca2+-switches in signaling networks detected by a planar plasmonic device. Anal Chem 84:2982–2989. https://doi.org/10.1021/ac300213j
12. Dizhoor AM, Olshevskaya EV, Peshenko IV (2010) Mg2+/Ca2+ cation binding cycle of guanylyl cyclase activating proteins (GCAPs): role in regulation of photoreceptor guanylyl cyclase. Mol Cell Biochem 334:117–124. https://doi.org/10.1007/s11010-009-0328-6
13. Marino V, Sulmann S, Koch KW, Dell'Orco D (1853) Structural effects of Mg(2)(+) on the regulatory states of three neuronal calcium sensors operating in vertebrate phototransduction. Biochim Biophys Acta 2055–2065:2015. https://doi.org/10.1016/j.bbamcr.2014.10.026
14. Peshenko IV, Dizhoor AM (2004) Guanylyl cyclase-activating proteins (GCAPs) are Ca2+/Mg2+ sensors: implications for photoreceptor guanylyl cyclase (RetGC) regulation in mammalian photoreceptors. J Biol Chem 279:16903–16906. https://doi.org/10.1074/jbc.C400065200
15. Marino V, Dell'Orco D (2016) Allosteric communication pathways routed by Ca(2+)/Mg(2+) exchange in GCAP1 selectively switch target regulation modes. Sci Rep 6:34277. https://doi.org/10.1038/srep34277
16. Koch KW, Duda T, Sharma RK (2010) Ca(2+)-modulated vision-linked ROS-GC guanylate cyclase transduction machinery. Mol Cell Biochem 334:105–115. https://doi.org/10.1007/s11010-009-0330-z
17. Biasi A et al (2021) A novel GUCA1A variant associated with cone dystrophy alters cGMP signaling in photoreceptors by strongly interacting with and hyperactivating retinal guanylate cyclase. Int J Mol Sci. https://doi.org/10.3390/ijms221910809
18. Dell'Orco D, Behnen P, Linse S, Koch KW (2010) Calcium binding, structural stability and guanylate cyclase activation in GCAP1 variants associated with human cone dystrophy. Cell Mol Life Sci 67:973–984. https://doi.org/10.1007/s00018-009-0243-8
19. Dizhoor AM, Boikov SG, Olshevskaya EV (1998) Constitutive activation of photoreceptor guanylate cyclase by Y99C mutant of GCAP-1. Possible role in causing human autosomal dominant cone degeneration. J Biol Chem 273:17311–17314. https://doi.org/10.1074/jbc.273.28.17311
20. Jiang L et al (2008) A novel GCAP1(N104K) mutation in EF-hand 3 (EF3) linked to autosomal dominant cone dystrophy. Vis Res 48:2425–2432. https://doi.org/10.1016/j.visres.2008.07.016
21. Kamenarova K et al (2013) Novel GUCA1A mutations suggesting possible mechanisms of pathogenesis in cone, cone-rod, and macular dystrophy patients. Biomed Res Int 2013:517570. https://doi.org/10.1155/2013/517570
22. Kitiratschky VB et al (2009) Mutations in the GUCA1A gene involved in hereditary cone dystrophies impair calcium-mediated regulation of guanylate cyclase. Hum Mutat 30:E782-796. https://doi.org/10.1002/humu.21055
23. Manes G et al (2017) Cone dystrophy or macular dystrophy associated with novel autosomal dominant GUCA1A mutations. Mol Vis 23:198–209
24. Marino V et al (2018) A novel p.(Glu111Val) missense mutation in GUCA1A associated with cone-rod dystrophy leads to impaired calcium sensing and perturbed second messenger homeostasis in photoreceptors. Hum Mol Genet 27:4204–4217. https://doi.org/10.1093/hmg/ddy311
25. Marino V, Scholten A, Koch KW, Dell'Orco D (2015) Two retinal dystrophy-associated missense mutations in GUCA1A with distinct molecular properties result in a similar aberrant regulation of the retinal guanylate cyclase. Hum Mol Genet 24:6653–6666. https://doi.org/10.1093/hmg/ddv370
26. Nishiguchi KM et al (2004) A novel mutation (I143NT) in guanylate cyclase-activating protein 1 (GCAP1) associated with autosomal dominant cone degeneration. Invest Ophthalmol Vis Sci 45:3863–3870. https://doi.org/10.1167/iovs.04-0590
27. Peshenko IV et al (2019) A G86R mutation in the calcium-sensor protein GCAP1 alters regulation of retinal guanylyl cyclase and causes dominant cone-rod degeneration. J Biol Chem 294:3476–3488. https://doi.org/10.1074/jbc.RA118.006180
28. Sokal I et al (2005) A novel GCAP1 missense mutation (L151F) in a large family with autosomal dominant cone-rod dystrophy (adCORD). Invest Ophthalmol Vis Sci 46:1124–1132. https://doi.org/10.1167/iovs.04-1431
29. Sokal I et al (1998) GCAP1 (Y99C) mutant is constitutively active in autosomal dominant cone dystrophy. Mol Cell 2:129–133. https://doi.org/10.1016/s1097-2765(00)80121-5
30. Vocke F et al (2017) Dysfunction of cGMP signalling in photoreceptors by a macular dystrophy-related mutation in the calcium sensor GCAP1. Hum Mol Genet 26:133–144. https://doi.org/10.1093/hmg/ddw374
31. Wilkie SE et al (2001) Identification and functional consequences of a new mutation (E155G) in the gene for GCAP1 that causes autosomal dominant cone dystrophy. Am J Hum Genet 69:471–480. https://doi.org/10.1086/323265

32. Gill JS, Georgiou M, Kalitzeos A, Moore AT, Michaelides M (2019) Progressive cone and cone-rod dystrophies: clinical features, molecular genetics and prospects for therapy. Br J Ophthalmol. https://doi.org/10.1136/bjophthalmol-2018-313278
33. Dell'Orco D, Dal Cortivo G (2019) Normal GCAPs partly compensate for altered cGMP signaling in retinal dystrophies associated with mutations in GUCA1A. Sci Rep 9:20105. https://doi.org/10.1038/s41598-019-56606-5
34. Vinberg F, Kefalov V (2015) Simultaneous ex vivo functional testing of two retinas by in vivo electroretinogram system. J Vis Exp. https://doi.org/10.3791/52855
35. Vinberg F, Koskelainen A (2010) Calcium sets the physiological value of the dominant time constant of saturated mouse rod photoresponse recovery. PLoS ONE 5:e13025. https://doi.org/10.1371/journal.pone.0013025
36. Liu P, Chen G, Zhang J (2022) A review of liposomes as a drug delivery system: current status of approved products, regulatory environments, and future perspectives. Molecules. https://doi.org/10.3390/molecules27041372
37. Wang N, Wang T, Li T, Deng Y (2009) Modulation of the physicochemical state of interior agents to prepare controlled release liposomes. Colloids Surf B Biointerfaces 69:232–238. https://doi.org/10.1016/j.colsurfb.2008.11.033
38. Cangiano L, Asteriti S (2023) An ex vivo electroretinographic apparatus for the ml-scale testing of drugs to one day and beyond. Int J Mol Sci. https://doi.org/10.3390/ijms241411346
39. Mandal A et al (2018) Ocular delivery of proteins and peptides: challenges and novel formulation approaches. Adv Drug Deliv Rev 126:67–95. https://doi.org/10.1016/j.addr.2018.01.008
40. Attia SA, MacKay JA (2022) Protein and polypeptide mediated delivery to the eye. Adv Drug Deliv Rev 188:114441. https://doi.org/10.1016/j.addr.2022.114441
41. El Sanharawi M et al (2010) Protein delivery for retinal diseases: from basic considerations to clinical applications. Prog Retin Eye Res 29:443–465. https://doi.org/10.1016/j.preteyeres.2010.04.001
42. Dawaliby R et al (2016) Phosphatidylethanolamine is a key regulator of membrane fluidity in eukaryotic cells. J Biol Chem 291:3658–3667. https://doi.org/10.1074/jbc.M115.706523
43. Hamano F et al (2021) Mapping membrane lipids in the developing and adult mouse retina under physiological and pathological conditions using mass spectrometry. J Biol Chem 296:100303. https://doi.org/10.1016/j.jbc.2021.100303
44. Agbaga MP et al (2018) Differential composition of DHA and very-long-chain PUFAs in rod and cone photoreceptors. J Lipid Res 59:1586–1596. https://doi.org/10.1194/jlr.M082495
45. Verra DM et al (2022) Intrinsic differences in rod and cone membrane composition: implications for cone degeneration. Graefes Arch Clin Exp Ophthalmol 260:3131–3148. https://doi.org/10.1007/s00417-022-05684-9
46. Moser T, Grabner CP, Schmitz F (2020) Sensory processing at ribbon synapses in the retina and the cochlea. Physiol Rev 100:103–144. https://doi.org/10.1152/physrev.00026.2018
47. Lewandowski D et al (2022) Dynamic lipid turnover in photoreceptors and retinal pigment epithelium throughout life. Prog Retin Eye Res 89:101037. https://doi.org/10.1016/j.preteyeres.2021.101037
48. Falsini B et al (2016) Nerve growth factor improves visual loss in childhood optic gliomas: a randomized, double-blind, phase II clinical trial. Brain 139:404–414. https://doi.org/10.1093/brain/awv366
49. Domenici L et al (2014) Rescue of retinal function by BDNF in a mouse model of glaucoma. PLoS ONE 9:e115579. https://doi.org/10.1371/journal.pone.0115579
50. Henderson JM, Zurzolo C (2021) Seeing eye to eye: photoreceptors employ nanotube-like connections for material transfer. EMBO J 40:e109727. https://doi.org/10.15252/embj.2021109727
51. Kalargyrou AA et al (2021) Nanotube-like processes facilitate material transfer between photoreceptors. EMBO Rep 22:e53732. https://doi.org/10.15252/embr.202153732
52. Heisterkamp P et al (2022) Evidence for endogenous exchange of cytoplasmic material between a subset of cone and rod photoreceptors within the adult mammalian retina via direct cell-cell connections. Exp Eye Res 219:109033. https://doi.org/10.1016/j.exer.2022.109033
53. Reid SN, Farber DB (2005) Glial transcytosis of a photoreceptor-secreted signaling protein, retinoschisin. Glia 49:397–406. https://doi.org/10.1002/glia.20131
54. Dell'Orco D, Sulmann S, Zagel P, Marino V, Koch KW (2014) Impact of cone dystrophy-related mutations in GCAP1 on a kinetic model of phototransduction. Cell Mol Life Sci 71:3829–3840. https://doi.org/10.1007/s00018-014-1593-4
55. Vighi E et al (2018) Combination of cGMP analogue and drug delivery system provides functional protection in hereditary retinal degeneration. Proc Natl Acad Sci U S A 115:E2997–E3006. https://doi.org/10.1073/pnas.1718792115
56. Asteriti S et al (2015) Effective delivery of recombinant proteins to rod photoreceptors via lipid nanovesicles. Biochem Biophys Res Commun 461:665–670. https://doi.org/10.1016/j.bbrc.2015.04.088
57. Beelen CJ, Asteriti S, Cangiano L, Koch KW, Dell'Orco D (2021) A hybrid stochastic/deterministic model of single photon response and light adaptation in mouse rods. Comput Struct Biotechnol J 19:3720–3734. https://doi.org/10.1016/j.csbj.2021.06.033
58. Sun YJ et al (2021) An intravitreal implant injection method for sustained drug delivery into mouse eyes. Cell Rep Methods. https://doi.org/10.1016/j.crmeth.2021.100125
59. Suh S, Choi EH, Raguram A, Liu DR, Palczewski K (2022) Precision genome editing in the eye. Proc Natl Acad Sci U S A 119:e2210104119. https://doi.org/10.1073/pnas.2210104119
60. Yan AL, Du SW, Palczewski K (2023) Genome editing, a superior therapy for inherited retinal diseases. Vision Res 206:108192. https://doi.org/10.1016/j.visres.2023.108192
61. Tuteja N (2009) Signaling through G protein coupled receptors. Plant Signal Behav 4:942–947. https://doi.org/10.4161/psb.4.10.9530
62. Hwang JY, Koch KW (2002) Calcium- and myristoyl-dependent properties of guanylate cyclase-activating protein-1 and protein-2. Biochemistry 41:13021–13028. https://doi.org/10.1021/bi026618y
63. Stephen R, Bereta G, Golczak M, Palczewski K, Sousa MC (2007) Stabilizing function for myristoyl group revealed by the crystal structure of a neuronal calcium sensor, guanylate cyclase-activating protein 1. Structure 15:1392–1402. https://doi.org/10.1016/j.str.2007.09.013
64. Hwang JY et al (2003) Regulatory modes of rod outer segment membrane guanylate cyclase differ in catalytic efficiency and Ca(2+)-sensitivity. Eur J Biochem 270:3814–3821. https://doi.org/10.1046/j.1432-1033.2003.03770.x
65. Zagel P, Dell'Orco D, Koch KW (2013) The dimerization domain in outer segment guanylate cyclase is a Ca(2)(+)-sensitive control switch module. Biochemistry 52:5065–5074. https://doi.org/10.1021/bi400288p
66. Tsien R, Pozzan T (1989) Measurement of cytosolic free Ca2+ with quin2. Methods Enzymol 172:230–262. https://doi.org/10.1016/s0076-6879(89)72017-6
67. Lange C, Koch KW (1997) Calcium-dependent binding of recoverin to membranes monitored by surface plasmon resonance spectroscopy in real time. Biochemistry 36:12019–12026. https://doi.org/10.1021/bi970938d
68. Asteriti S, Ricci V, Cangiano L (2020) Two simple criteria to estimate an objective's performance when imaging

in non design tissue clearing solutions. J Neurosci Methods 332:108564. https://doi.org/10.1016/j.jneumeth.2019.108564
69. Asteriti S, Cangiano L (2020) Versatile bipolar temperature controller for custom in vitro applications. HardwareX 8:e00155. https://doi.org/10.1016/j.ohx.2020.e00155